

Extremal-point densities of interface fluctuations

Z. Toroczkai,^{1,4} G. Korniss,³ S. Das Sarma,¹ and R. K. P. Zia²

¹*Department of Physics, University of Maryland, College Park, Maryland 20742-4111*

²*Department of Physics, Virginia Polytechnic Institute and State University, Blacksburg, Virginia 24061-0435*

³*Supercomputer Computations Research Institute, Florida State University, Tallahassee, Florida 32306-4130*

⁴*Center for Nonlinear Science and Theoretical Division, Los Alamos National Laboratory, Los Alamos, New Mexico 87544*

(Received 16 February 2000)

We introduce and investigate the stochastic dynamics of the density of local extrema (minima and maxima) of nonequilibrium surface fluctuations. We give a number of analytic results for interface fluctuations described by linear Langevin equations, and for on-lattice, solid-on-solid surface-growth models. We show that, in spite of the nonuniversal character of the quantities studied, their behavior against the variation of the microscopic length scales can present generic features, characteristic of the macroscopic observables of the system. The quantities investigated here provide us with tools that give an unorthodox approach to the dynamics of surface morphologies: a statistical analysis from the short-wavelength end of the Fourier decomposition spectrum. In addition to surface-growth applications, our results can be used to solve the asymptotic scalability problem of massively parallel algorithms for discrete-event simulations, which are extensively used in Monte Carlo simulations on parallel architectures.

PACS number(s): 05.40.-a, 02.50.-r, 05.45.Df, 68.35.Ct

I. INTRODUCTION AND MOTIVATION

The aim of statistical mechanics is to relate macroscopic observables to the microscopic properties of the system. Before attempting such derivation, one always has to specify the spectrum of length scales the analysis will comprise: while “macroscopic” is usually defined in a unique way by the everyday-life length scale, the “microscopic” is never so obvious, and the choice of the best lower-end scale is highly nonuniversal. It is system dependent, usually left to our physical “intuition,” or it is set by the limitations of the experimental instrumentation. It is obvious that in order to derive the laws of gaseous matter we do not need to employ the physics of elementary particles; it is enough to start from an effective microscopic model (or Hamiltonian) on the level of molecular interactions. Then starting from the equations of motion on the microscopic level and using a statistical and probabilistic approach, the macroscale physics is derived. In this “long-wavelength” approach most of the microscopic or short-wavelength information is usually redundant, and it is scaled away.

Sometimes, however, microscopic quantities are important and directly contribute to macroscopic observables, e.g., the nearest-neighbor correlations in driven systems determine the current, in phase separation with conserved order parameter (model B) the mobility, in kinetic Ising models the domain-wall velocity, in parallel computation the utilization (efficiency) of conservative parallel algorithms, etc. Once a lower length scale is set, on which we can define an effective microscopic dynamics, it becomes meaningful to ask questions about local properties *at this length scale*, e.g., nearest-neighbor correlations, contour distributions, extremal-point densities, etc. These quantities are obviously not universal. However, their *behavior* against the variation of the length scales can present qualitative and universal features [1]. Here we study the dynamics of macroscopically rough surfaces by investigating an intriguing microscopic quantity: the density of extrema (local minima) and its finite-size effects. We de-

rive a number of analytical results about these quantities for a large class of nonequilibrium surface fluctuations described by linear Langevin equations and solid-on-solid (SOS) lattice-growth models. Besides its obvious relevance to surface physics, our technique can be used to show [2] the asymptotic scalability of conservative massively parallel algorithms for discrete-event simulation, i.e., the fact that the *efficiency* of such computational schemes does not vanish with increasing number of processing elements. Rather, it has a nontrivial lower bound. The solution of this problem not only is of practical importance from the point of view of parallel computing, but has important consequences for our understanding of systems with *asynchronous* parallel dynamics in general. There are numerous dynamical systems, both artificial and found in nature, that contain a “substantial amount” of parallelism, like the following examples.

(1) In wireless cellular communications the call arrivals and departures are occurring in continuous time (Poisson arrivals), and the discrete events (call arrivals) are *not* synchronized by a global clock. Nevertheless, calls initiated in cells substantially far from each other can be processed simultaneously by the parallel simulator *without* changing the Poissonian nature of the underlying process. The problem of designing efficient dynamic channel allocation schemes for wireless networks is a very difficult one, and currently it is done by modeling the network as a system of interacting continuous-time stochastic automata on parallel architectures [3].

(2) In magnetic systems the discrete events are the spin-flip attempts (e.g., Glauber dynamics for Ising systems). While traditional single-spin-flip dynamics may seem inherently serial, systems with short-range interactions can be simulated in parallel: spins sufficiently far from each other with *different* local simulated times can be updated simultaneously. Fast and efficient parallel Monte Carlo algorithms are extremely welcome when studying metastable decay and hysteresis of kinetic Ising ferromagnets below their critical temperature; see [4] and references therein.

(3) Financial markets, and especially the stock market, are an extremely dynamic, high-connectivity network of relations: thousands of trades are being made asynchronously every minute [5].

(4) The human brain, in spite of its low weight of approximately 1 kg and volume of 1400 cm³, contains about 100 billion neurons, each neuron being connected through synapses to approximately 10 000 other neurons. The total number of synapses in a human brain is about 1000 trillion (10¹⁵). The neurons of a single human brain, placed end to end, would make a “string” of an enormous length: 250 000 miles [6]. Assuming that each neuron of a single human cortex can be in two states only (resting or acting), the total number of different brain configurations would be 2^{10¹¹}. According to Carl Sagan, this number is greater than the total number of protons and electrons of the known Universe [6]. The brain does an incredible amount of parallel computation: it simultaneously manages all of our body functions, we can talk and walk at the same time, etc.

(5) Evolution of networks such as the internet has asynchronous parallel dynamics: the local network connectivity changes “concurrently” (within a small time interval) as many sites are attached or removed in different locations. As a matter of fact, the physics of such dynamic networks is currently a heavily investigated and rapidly emerging field [7].

In order to present the basic ideas and notions in the simplest way, in the following we restrict ourselves to one-dimensional interfaces that have no overhangs. The restriction on overhangs may actually be lifted with a proper parametrization of the surface, a problem to which we will return briefly in the concluding section. The first visual impression when one looks at a rough surface $h(x,t)$ is the extent of the fluctuations perpendicular to the substrate, in other words, the *width* of the interface. The width (or the rms of the height h of the fluctuations) is probably the most extensively studied quantity in interface physics, due to the fact that its definition is simply quantifiable and therefore measurable:

$$w(L,t) = \sqrt{[\overline{h(x,t)}]^2 - [\overline{h(x,t)}]^2}, \quad (1)$$

where the overbar denotes an average over the substrate. It is well known that this quantity characterizes the long-wavelength behavior of the fluctuations, the high-frequency components being averaged out in Eq. (1). The short-wavelength end of the spectrum has been ignored in the literature mainly because of its nonuniversal character, and also because it seemed to lack such a simple quantifiable definition as the width w .

In the following we present a quantity that is almost as simple and intuitive as the width w , but characterizes the high-frequency components of the fluctuations. For illustrative purposes, let us consider the classic Weierstrass function defined as the $M \rightarrow \infty$ limit of the smooth functions $W_M(a,b;x)$:

$$\begin{aligned} W(a,b;x) &= \lim_{M \rightarrow \infty} W_M(a,b;x) \\ &= \lim_{M \rightarrow \infty} \sum_{m=0}^M a^{-m} \cos(b^m x), \quad a,b > 1. \end{aligned} \quad (2)$$

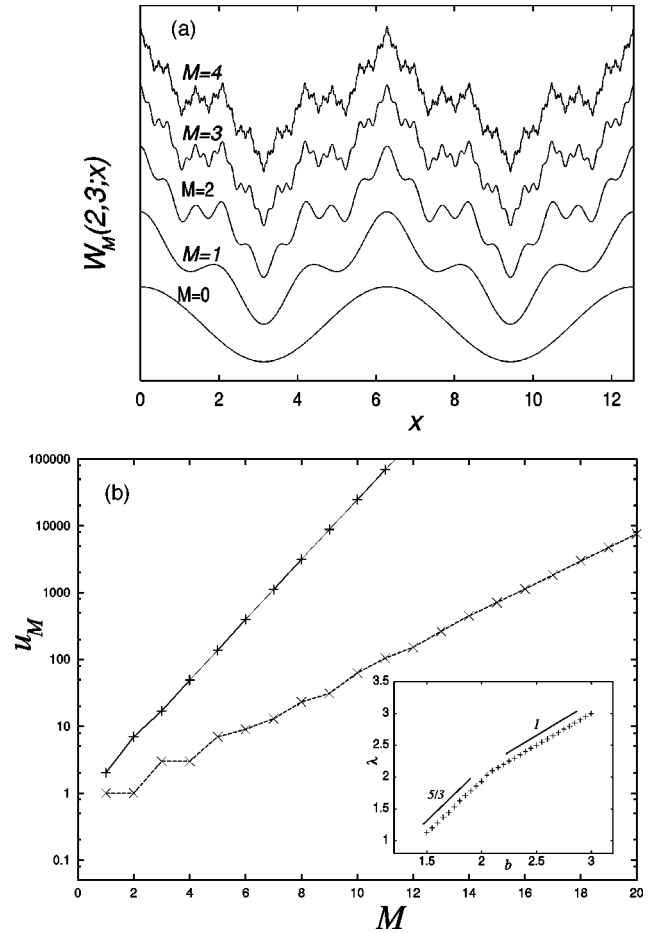


FIG. 1. (a) The function $W_M(a,b;x)$ at $a=2$, $b=3$, and $M=0,1,2,3,4$. (b) The scaling of the number of local minima $u_M \sim \lambda^M$ for $b=2.8$ (pluses) and $b=1.8$ (crosses). The inset shows λ vs b while keeping a constant, $a=2$. The solid lines indicate the slopes $5/3$ and 1 , respectively.

Figure 1(a) shows the graph of W_M at $a=2$ and $b=3$ (arbitrary values) for $M=0,1,2,3,4$ in the interval $x \in [0,4\pi]$. As one can see, by increasing M we are adding more and more detail to the graph of the function on finer and finer length scales. Thus, M plays the role of a regulator for the microscopic cutoff length which is b^{-M} , and for $M=\infty$ and $b > a$, the function becomes nowhere differentiable as was shown by Hardy [8].

Comparing the graphs of W_M for lower M values with those for higher M we observe that the width effectively does not change; however, the curves look qualitatively very different. This is obvious from Eq. (2): adding an extra term does not change the long-wavelength modes, but adds a higher-frequency component to the Fourier spectrum of the graph. We need to operationally define a quantity that makes a distinction between a much “fuzzier” graph, such as for $M=4$, and a smoother one, such as for $M=1$. The natural choice based on Fig. 1(a) is the *number of local minima* (or extrema) in the graph of the function. In Fig. 1(b) we present the number of local minima u_M vs M for two different values of b , $b=2.8$ and $b=1.8$, while keeping a at the same value of $a=2$. For all b values (not only for these two) the leading behavior is exponential: $u_M \sim \lambda^M$. The inset in Fig. 1(b) shows the dependence of the rate λ as a function of b for

fixed a . We observe that for $b > a$, $\lambda = b$, but below $b = a$ the dependence crosses over to another, seemingly linear function. For $b > a$ the amplitude of the extra added term in W_{M+1} is large enough to prevent the cancellation of the newly appearing minima by the drop in the local slope of W_M . At $b \leq a$ the number of canceled extrema starts to increase drastically with an exponential trend, leading to the crossover seen in the inset of Fig. 1(b). It has been shown that the fractal dimension of the Weierstrass function for $b > a$ is given by $D_0 = \ln b / \ln a$ [9,10]. For $b \leq a$ the Weierstrass curve becomes nonfractal with a dimension of $D_0 = 1$. By varying b with respect to a , we are crossing a fractal-smooth transition at $b = a$. The very intriguing observation we have just come across is that, even though we are in the smooth regime ($b < a$), the density of minima is still a *diverging* quantity [the $b = 1.8$ curve in Fig. 1(b)]. It is thus possible to have an infinite number of “wrinkles” in the Weierstrass function without having a diverging length, without having a fractal in the classical sense. The transition from fractal to smooth as b is lowered appears as a nonanalyticity in the divergence rate of the curve’s wrinkledness. A rigorous analytic treatment of this problem seems to be highly nontrivial, and we propose it as an open question to the interested reader.

The simple example above shows that there is interesting and nontrivial physics lying behind the analysis of extremal-point densities, and it gives extra information on the morphology of interfaces. Given an interface $h(x, t)$, we propose a quantitative form that characterizes the density of minima via a “partition-function-like” expression, which is hardly more complex than Eq. (1) and gives an alternate description of the surface morphology:

$$u_q(L, [h]) = \frac{1}{L} \sum_i [K(x_i)]^q, \quad q > 0, \quad (3)$$

x_i are nondegenerate minima of h ,

with $K(x_i)$ denoting the *curvature* of h at the local (nondegenerate) minimum point x_i . The variable q can be conceived as an inverse temperature. Obviously, for $q = 0$ we obtain the number of local minima per unit interface length. The rigorous mathematical description and definitions lying at the basis of Eq. (3) are presented in Sec. IV. The quantity in Eq. (3) is reminiscent of the partition function used in the definition of the thermodynamical formalism of one-dimensional chaotic maps [11], and also of the definition of the dynamical or Rényi entropies of these chaotic maps. In that case, however, the curvatures at the minima are replaced by cylinder intervals and/or the visiting probabilities of these cylinders.

We present a detailed analysis of the above quantity for a large class of linear Langevin equations of type $\partial h / \partial t = -\nu(-\nabla^2 h)^{z/2} + \eta(x, t)$, where η is a Gaussian noise term and z a positive real number. These Langevin equations are found to describe faithfully the fluctuations of monatomic steps on various substrates (for a review, see Ref. [12]). One of the interesting conclusions we came to by studying the extremal-point densities for such equations is that, depending on the value of z , the typical surface morphology can be fractal, or locally smooth, and the two regimes are separated

by a critical z value, z_c . In the fractal case, the interface has infinitely many minima and cusps, just as in the case of the nondifferentiable Weierstrass function (2), and the extremal-point densities become infinite. (If the problem is discretized onto a lattice with spacing a , a power-law diverging behavior is observed for these densities as $a \rightarrow 0^+$.) This sudden change of the “intrinsic roughness” may be conceived as a phase transition, even in an experimental situation. On changing a parameter, such as the temperature, the *law* describing the fluctuations can change since the mechanism responsible for the fluctuations can change character as the temperature varies. For example, it has been recently shown using scanning tunneling microscope measurements [13] that the fluctuations of single-atom-layer steps on Cu(111) below $T = 300^\circ\text{C}$ correspond to the periphery diffusion mechanism ($z = 4$), but above this temperature (such as $T = 500^\circ\text{C}$ in these measurements) the mechanism is attachment-detachment, for which $z = 2$ (see also Refs. [14,15]).

The paper is organized as follows. In Secs. II and III we define and investigate the minimum-point density for several well-known on-lattice models, and derive exact results in the steady state ($t \rightarrow \infty$), including finite-size effects. As a practical application of these on-lattice results, we briefly present in Sec. III B a lattice surface-growth model that exactly describes the evolution of the simulated time horizon for conservative massively parallel schemes in parallel computation, solving a long-standing asymptotic scalability question for these update schemes. In Sec. IV we lay down a more rigorous mathematical treatment for extremal-point densities, and stochastic extremal-point densities on the continuum, with a detailed derivation for a large class of linear Langevin equations (which are in fact the continuum counterparts of the discrete ones from Sec. II). The more rigorous treatment allows for an exact analytical evaluation not only in the steady state, but for all times. We identify characteristic exponents that separate regimes with divergent extremal-point densities from convergent ones, and which give insight into the short-wavelength physics behind these kinetic roughening processes.

II. LINEAR SURFACE-GROWTH MODELS ON THE LATTICE

In the present section we focus on discrete, one-dimensional models from the linear theory of kinetic roughening [16,17]. Let us consider a one-dimensional substrate consisting of L lattice sites with periodic boundary conditions. For simplicity the lattice constant is taken as unity, which clearly represents the lower cutoff length for the effective equation of motion. For the moment let us study the general Langevin equation on a lattice that describes the linear theory of molecular beam epitaxy (MBE) [18,19]:

$$\partial_t h_i(t) = \nu \nabla^2 h_i(t) - \kappa \nabla^4 h_i(t) + \eta_i(t), \quad (4)$$

where $\eta_i(t)$ is Gaussian white noise with

$$\langle \eta_i(t) \eta_j(t') \rangle = 2D \delta_{i,j} \delta(t - t'), \quad (5)$$

and ∇^2 is the discrete Laplacian operator, i.e., $\nabla^2 f_j = f_{j+1} + f_{j-1} - 2f_j$, applied to an arbitrary lattice function f_j . This equation arises in MBE with both surface diffusion (the

fourth-order or curvature term) and desorption (the second-order or diffusive term), and it has been studied extensively by several authors [18,20]. Since we will study both $\kappa \rightarrow 0$ and $\nu \rightarrow 0$ limiting cases, generic stability requires $\nu \geq 0$ and $\kappa \geq 0$. Starting from a completely flat initial condition, the interface roughens until the correlation length ξ reaches the size of the system $\xi \approx L$, when the roughening saturates and the system enters a steady-state regime. The process of kinetic roughening is controlled by the intrinsic length scale $\sqrt{\kappa/\nu}$ [20]. Below this length scale the roughening is dominated by the surface diffusion or Mullins [21] term (the fourth-order operator), while above it is characterized by the evaporation term (the diffusion) or Edwards-Wilkinson (EW) [22] term. Since Eq. (4) is translationally invariant and linear in h , it can be solved via the discrete Fourier transform

$$\tilde{h}_k = \sum_{j=0}^{L-1} e^{-ikj} h_j, \quad k = \frac{2\pi n}{L}, \quad n=0,1,2,\dots,L-1. \quad (6)$$

Then Eq. (4) translates into

$$\partial_t \tilde{h}_k(t) = -\{2\nu[1 - \cos(k)] + 4\kappa[1 - \cos(k)]^2\} \tilde{h}_k(t) + \tilde{\eta}_k(t), \quad (7)$$

with

$$\langle \tilde{\eta}_k(t) \tilde{\eta}_{k'}(t') \rangle = 2DL \delta_{(k+k') \bmod 2\pi, 0} \delta(t-t'). \quad (8)$$

Following the definition of the equal-time structure factor $S^h(k, t)$, namely,

$$S^h(k, t) L \delta_{(k+k') \bmod 2\pi, 0} \equiv \langle \tilde{h}_k(t) \tilde{h}_{k'}(t) \rangle, \quad (9)$$

one obtains for an initially flat interface

$$S^h(k, t) = S^h(k) (1 - e^{-\{4\nu[1 - \cos(k)] + 8\kappa[1 - \cos(k)]^2\}t}). \quad (10)$$

In the above equation,

$$S^h(k) \equiv \lim_{t \rightarrow \infty} S^h(k, t) = \frac{D}{2\nu[1 - \cos(k)] + 4\kappa[1 - \cos(k)]^2} \quad (11)$$

is the steady-state structure factor.

For $\nu \neq 0$, and in the asymptotic scaling limit where $L \gg \sqrt{\kappa/\nu}$, the model belongs to the EW universality class and the roughening exponent is $\alpha = 1/2$ (it is defined through the scaling $L^{2\alpha}$ of the interface width $\langle w_L^2(t) \rangle = (1/L) \langle \sum_{i=1}^L [h_i(t) - \bar{h}]^2 \rangle$ in the steady state). The presence of the curvature term does not change the universal scaling properties for the surface width, and one finds the same exponents as for the pure EW case ($\kappa = 0$) in Eq. (4). For $\nu = 0$ the surface is purely curvature driven ($z = 4$) and the model belongs to a different universality class where the steady-state width scales with a roughness exponent of $\alpha = 3/2$.

In the following we will be mostly interested in some local steady-state properties of the surface h_i . In particular,

we want to find the density of local minima for the surface described by Eq. (4). The operator that measures this quantity is

$$u = \frac{1}{L} \sum_{i=1}^L \Theta(h_{i-1} - h_i) \Theta(h_{i+1} - h_i). \quad (12)$$

This expression motivates the introduction of the local slopes $\phi_i = h_{i+1} - h_i$. In this representation the operator for the density of local minima (for the original surface) is

$$u = \frac{1}{L} \sum_{i=1}^L \Theta(-\phi_{i-1}) \Theta(\phi_i), \quad (13)$$

and its steady-state average is $\langle u \rangle = \langle \Theta(-\phi_{i-1}) \Theta(\phi_i) \rangle = \langle \Theta(-\phi_1) \Theta(\phi_2) \rangle$, due to translational invariance. The average density of local minima is the same as the probability that a randomly chosen site of the lattice corresponds to a local minimum of the surface. It is governed by the nearest-neighbor two-slope distribution, which is also Gaussian and fully determined by $\langle \phi_1^2 \rangle = \langle \phi_2^2 \rangle$ and $\langle \phi_1 \phi_2 \rangle$:

$$P^{\text{nn}}(\phi_1, \phi_2) \propto e^{-\phi_j A_{jk}^{\text{nn}} \phi_k / 2}, \quad j, k = 1, 2, \quad (14)$$

where

$$A^{\text{nn}} = \begin{pmatrix} \langle \phi_1^2 \rangle & \langle \phi_1 \phi_2 \rangle \\ \langle \phi_1 \phi_2 \rangle & \langle \phi_2^2 \rangle \end{pmatrix}^{-1}. \quad (15)$$

As we show in Appendix A, the density of local minima depends only on the ratio $\langle \phi_1 \phi_2 \rangle / \langle \phi_1^2 \rangle$:

$$\langle u \rangle = \frac{1}{2\pi} \arccos \left(\frac{\langle \phi_1 \phi_2 \rangle}{\langle \phi_1^2 \rangle} \right). \quad (16)$$

Finite-size effects in $\langle u \rangle$ are obviously carried through from the correlations. First we find the steady-state structure factor for the slopes. Since $\tilde{\phi}_k = (1 - e^{-ik}) \tilde{h}_k$, we have $S^\phi(k) = 2[1 - \cos(k)] S^h(k)$. Then from Eq. (11) one obtains

$$S^\phi(k) = \frac{D}{\nu + 2\kappa[1 - \cos(k)]} \quad \text{for } k \neq 0$$

and

$$S^\phi(k) = 0 \quad \text{for } k = 0. \quad (17)$$

The latter automatically follows from the $\sum_{i=1}^L \phi_i = 0$ relation. Then we obtain the slope-slope correlations

$$C_L^\phi(l) \equiv \langle \phi_i \phi_{i+l} \rangle = \frac{1}{L} \sum_{n=1}^{L-1} e^{i(2\pi n/L)l} S^\phi \left(\frac{2\pi n}{L} \right). \quad (18)$$

With the help of Poisson summation formulas, in Appendix B we show a derivation for the exact spatial correlation function, which yields

$$C_L^\phi(l) = \frac{D}{\nu+2\kappa} \left(\frac{b^{|l|}}{\sqrt{1-a^2}} - \frac{1}{1-a} \frac{1}{L} + \frac{b^L}{1-b^L} \frac{b^l + b^{-l}}{\sqrt{1-a^2}} \right), \quad |l| \leq L, \quad (19)$$

with

$$a \equiv \frac{2\kappa}{\nu+2\kappa} \quad \text{and} \quad b \equiv \frac{1-\sqrt{1-a^2}}{a}. \quad (20)$$

We have $|a| \leq 1$ and $b \leq 1$. The second term in the parentheses in Eq. (19) gives a *uniform* power-law correction, while the third one gives an exponential correction to the correlation function in the thermodynamic limit. For $\nu \neq 0$ and $L \rightarrow \infty$ one obtains

$$C_\infty^\phi(l) = \frac{D}{\nu+2\kappa} \frac{b^{|l|}}{\sqrt{1-a^2}} = \frac{D}{\nu+2\kappa} \frac{e^{-|l|/\xi_\infty^\phi}}{\sqrt{1-a^2}}, \quad (21)$$

where we define the correlation length of the slopes for an infinite system as

$$\xi_\infty^\phi \equiv -\frac{1}{\ln(b)}. \quad (22)$$

In the $\nu \rightarrow 0$ limit it becomes the intrinsic correlation length, which diverges as $\nu^{-1/2}$:

$$\xi_\infty^\phi \stackrel{\nu \rightarrow 0}{\approx} \sqrt{\kappa/\nu}$$

and

$$C_\infty^\phi(l) \stackrel{\nu \rightarrow 0}{\approx} \frac{D}{2\kappa} \left(\sqrt{\frac{\kappa}{\nu}} - |l| \right) \approx \frac{D}{2\kappa} (\xi_\infty^\phi - |l|). \quad (23)$$

In this limit the slopes (separated by any finite distance) become highly correlated, and one may start to anticipate that the density of local minima will vanish for the original surface $\{h_i\}$. In the following two subsections we investigate the density of local minima and its finite-size effects for the Edwards-Wilkinson and Mullins cases.

A. Density of local minima for the Edwards-Wilkinson regime

To study the finite-size effects for the local minimum density, we neglect the exponentially small correction in Eq. (19), so in the *asymptotic* limit, where $L \gg \xi_\infty^\phi$, $C_L^\phi(l)$ decays exponentially with *uniform* finite-size corrections:

$$C_L^\phi(l) \approx \frac{D}{\nu+2\kappa} \left(\frac{b^{|l|}}{\sqrt{1-a^2}} - \frac{1}{1-a} \frac{1}{L} \right). \quad (24)$$

This holds for the special case $\kappa=0$ as well (in fact, there the exponential correction exactly vanishes), leaving

$$C_L^\phi(l) = \frac{D}{\nu} \left(\delta_{l,0} - \frac{1}{L} \right). \quad (25)$$

Now, employing Eq. (16), we can obtain the density of minima as

$$\begin{aligned} \langle u \rangle_L &= \frac{1}{2\pi} \arccos \left(\frac{C_L^\phi(1)}{C_L^\phi(0)} \right) \\ &\approx \frac{1}{2\pi} \arccos(b) + \frac{1}{2\pi} \sqrt{\frac{1-b}{1+b}} \sqrt{\frac{1+a}{1-a}} \frac{1}{L}, \end{aligned} \quad (26)$$

Again, for the $\kappa=0$ case one has a compact exact expression and the corresponding large- L behavior:

$$\langle u \rangle_L = \frac{1}{2\pi} \arccos \left(-\frac{1}{L-1} \right) \approx \frac{1}{4} + \frac{1}{2\pi} \frac{1}{L}, \quad (27)$$

which can also be obtained by taking the $\kappa \rightarrow 0$ limit in Eq. (26). To summarize, as long as $\nu \neq 0$, the model belongs to the EW universality class, and in the steady state, the density of local minima behaves as

$$\langle u \rangle_L \approx \langle u \rangle_\infty + \frac{\text{const}}{L}, \quad (28)$$

where $\langle u \rangle_\infty$ is the value of the density of local minima in the thermodynamic limit:

$$\langle u \rangle_\infty = \frac{1}{2\pi} \arccos(b). \quad (29)$$

Note that this quantity can be small, but does not vanish if ν is close but not equal to 0. Further, the system exhibits the scaling (28) for asymptotically large systems, where $L \gg \xi_\infty^\phi$. It is important to see in detail how $\langle u \rangle_\infty$ behaves as $\nu \rightarrow 0$:

$$\begin{aligned} \langle u \rangle_\infty &\stackrel{\nu \rightarrow 0}{\approx} \frac{1}{2\pi} \arccos(1 - \sqrt{2} \sqrt{1-a}) \\ &\approx \frac{1}{2\pi} \arccos \left(1 - \sqrt{\frac{\nu}{\kappa}} \right) \\ &\approx \frac{1}{2\pi} \left(2 \sqrt{\frac{\nu}{\kappa}} \right)^{1/2} \approx \frac{\sqrt{2}}{2\pi} \frac{1}{\sqrt{\xi_\infty^\phi}}. \end{aligned} \quad (30)$$

Thus, the density of local minima for an *infinite* system vanishes as we approach the purely curvature-driven ($\nu \rightarrow 0$) limit. Simply speaking, the local slopes become ‘‘infinitely’’ correlated, such that $C_\infty^\phi(l)$ diverges [according to Eq. (23)], and the ratio $C_\infty^\phi(l)/C_\infty^\phi(0)$ for any fixed l tends to 1. This is the physical picture behind the vanishing density of local minima.

B. Density of local minima for the Mullins regime

Here we take the $\nu \rightarrow 0$ limit *first* and then study the finite-size effects in the purely curvature-driven model. The slope correlations are finite for finite L , as can be seen from Eq. (18), since the $n=0$ term is not included in the sum. Thus, in the exact closed formula (19) a careful limiting procedure has to be taken, which indeed yields the internal cancellation of the apparently divergent terms. Then one obtains the exact slope correlations for the $\nu=0$ case,

$$C_L^\phi(l) = \frac{D}{2\kappa} \left[\frac{L}{6} \left(1 - \frac{1}{L^2} \right) - |l| \left(1 - \frac{|l|}{L} \right) \right], \quad (31)$$

and for the local minimum density,

$$\langle u \rangle_L = \frac{1}{2\pi} \arccos \left(1 - \frac{6}{L+1} \right) \simeq \frac{\sqrt{3}}{\pi} \frac{1}{\sqrt{L}}. \quad (32)$$

It vanishes in the thermodynamic limit, and hence one observes that the limits $\nu \rightarrow 0$ and $L \rightarrow \infty$ are interchangeable. For $\nu = 0$, L is directly associated with the correlation length and we can define $\xi_L^\phi \equiv L/6$. Then the correlations and the density of local minima take the same scaling form as Eqs. (23) and (30):

$$C_L^\phi(l) \simeq \frac{D}{2\kappa} (\xi_L^\phi - |l|) \quad (33)$$

and

$$\langle u \rangle_L \simeq \frac{\sqrt{2}}{2\pi} \frac{1}{\sqrt{\xi_L^\phi}}. \quad (34)$$

C. Scaling considerations for higher-order equations

Let us now consider another equation with a generalized relaxational term that includes the Edwards-Wilkinson and the noisy Mullins equation as particular cases:

$$\partial_t h_i(t) = -\nu (-\nabla^2)^{z/2} h_i(t) + \eta_i(t) \quad (35)$$

where z is a positive real number (not necessarily integer). Other z values of experimental interest are $z = 1$ (relaxation through plastic flow [17,21]) and $z = 3$ (terrace-diffusion mechanism [12,14,15]). For early times, such that $t \ll L^z$, the interface width $\langle w_L^2(t) \rangle$ increases with time as

$$\langle w_L^2(t) \rangle \sim t^{2\beta}, \quad (36)$$

where $\beta = (z-1)/2z$ [16,17]. In the $t \rightarrow \infty$ limit, where $t \gg L^z$, the interface width saturates for a finite system, but diverges with L according to $\langle w_L^2(\infty) \rangle \sim L^{2\alpha}$ where $\alpha = (z-1)/2$ is the roughness exponent [16,17].

For $z = 4$ (curvature-driven interface) we saw that the slope fluctuation behaves as $C_L^\phi(0) = \langle \phi_i^2 \rangle \sim L$. For higher z the slope-slope correlation function can be obtained as

$$C_L^\phi(l) = \frac{D}{L} \sum_{n=1}^{L-1} \frac{e^{i(2\pi n/L)l}}{\nu \{2[1 - \cos(2\pi n/L)]\}^{(z-2)/2}}. \quad (37)$$

It is divergent in the $L \rightarrow \infty$ limit, as a result of infinitely small wave vectors $\sim 2\pi/L$, and we can see that

$$C_L^\phi(0) \sim L^{z-3}. \quad (38)$$

It is also useful to define the slope-difference correlation function

$$G_L^\phi(l) \equiv \langle (\phi_{i+l} - \phi_i)^2 \rangle, \quad (39)$$

for which one can write

$$G_L^\phi(l) = \frac{D}{L} \sum_{n=1}^{L-1} \frac{2\{1 - \cos[(2\pi n/L)l]\}}{\nu \{2[1 - \cos(2\pi n/L)]\}^{(z-2)/2}}. \quad (40)$$

For small wave vectors we can again deduce that for $z > 5$

$$G_L^\phi(l) \sim L^{z-5} l^2. \quad (41)$$

One may refer to this form as ‘‘anomalous’’ scaling [17] for the slope-difference correlation function in the following sense. For $z < 5$ the scaling form for $G_L^\phi(l)$ follows that of $C_L^\phi(0)$ [Eq. (38)], i.e., $G_L^\phi(l) \sim l^{z-3}$. For $z > 5$ [Eq. (41)] it obviously features a different l dependence and an additional power of L , and it diverges in the $L \rightarrow \infty$ limit.

Having these scaling functions for large L , we can easily obtain the scaling behavior for the average density of local minima. Exploiting the identity

$$C_L^\phi(l) = C_L^\phi(0) - \frac{1}{2} G_L^\phi(l), \quad (42)$$

we use the general form for the local minimum density:

$$\begin{aligned} \langle u \rangle &= \frac{1}{2\pi} \arccos \left(\frac{C_L^\phi(1)}{C_L^\phi(0)} \right) \\ &= \frac{1}{2\pi} \arccos \left(1 - \frac{1}{2} \frac{G_L^\phi(1)}{C_L^\phi(0)} \right) \\ &\simeq \frac{1}{2\pi} \arccos \left(1 - \frac{\text{const}}{L^2} \right) \sim \frac{1}{L}. \end{aligned} \quad (43)$$

Note that this is the scaling behavior for *all* $z > 5$. It simply shows the trivial lower bound for $\langle u \rangle$: since there is always at least one minimum (and one maximum) among the L sites, it can never be smaller than $1/L$.

D. The average curvature at local minima

The next natural question to ask is how the average curvature K at the minimum points scales with the system size for the general system described by Eq. (35). This can be evaluated as the conditional average of the local curvature at the local minima:

$$\begin{aligned} \langle K \rangle_{\min} &= \langle (\phi_i - \phi_{i-1}) \rangle_{\min} \\ &= \frac{\langle (\phi_i - \phi_{i-1}) \Theta(-\phi_{i-1}) \Theta(\phi_i) \rangle}{\langle \Theta(-\phi_{i-1}) \Theta(\phi_i) \rangle} \\ &= \frac{\langle (\phi_2 - \phi_1) \Theta(-\phi_1) \Theta(\phi_2) \rangle}{\langle u \rangle}, \end{aligned} \quad (44)$$

where translational invariance is exploited again. The numerator in Eq. (44) can be obtained after performing the same basis transformation (Appendix A) that was essential to find $\langle u \rangle$. Then, after elementary integrations, we find

$$\begin{aligned} \langle K \rangle_{\min} &= \frac{1}{\langle u \rangle} \frac{1}{\sqrt{2\pi}} \frac{C_L^\phi(0) - C_L^\phi(1)}{\sqrt{C_L^\phi(0)}} \\ &= \frac{\sqrt{2\pi}}{\sqrt{C_L^\phi(0)}} \frac{C_L^\phi(0) - C_L^\phi(1)}{\arccos[C_L^\phi(1)/C_L^\phi(0)]}. \end{aligned} \quad (45)$$

Using the explicit results for the slope correlation function for $z=2$ and $z=4$ and its scaling forms for higher z given in the previous subsections, one can easily deduce the following. For $z < 5$ the average curvature at the local minimum points *on a lattice* tends to a *constant* in the thermodynamic limit. For $z=2$

$$\langle K \rangle_{\min} \simeq \frac{2\sqrt{2}}{\sqrt{\pi}} \sqrt{\frac{D}{\nu}} + O\left(\frac{1}{L}\right), \quad (46)$$

and for $z=4$

$$\langle K \rangle_{\min} \simeq \sqrt{\pi} \sqrt{\frac{D}{2\nu}} + O\left(\frac{1}{L}\right). \quad (47)$$

The behavior of this quantity drastically changes for $z > 5$, where it *diverges* with the system size as

$$\langle K \rangle_{\min} \sim L^{(z-5)/2}. \quad (48)$$

III. OTHER LATTICE MODELS AND AN APPLICATION TO PARALLEL COMPUTING

A. The single-step model

In the single-step model the height differences (i.e., the local slopes) are restricted to ± 1 , and the evolution consists of particles of height 2 being deposited at the local minima. While the full dynamic behavior of the model belongs to the Kardar-Parisi-Zhang (KPZ) universality class [23], in one dimension the steady state is governed by the EW Hamiltonian [24]. Thus, the roughness exponent is $\alpha=1/2$, and we expect the finite-size effects for $\langle u \rangle$ to follow Eq. (28). The advantage of this model is that it can be mapped onto a driven hard-core lattice gas for which the *steady-state* probability distribution of the configurations is known exactly [24,25] (each configuration has equal weight). This enables us to find arbitrary moments of the local minimum density operator. Since $\phi_i = \pm 1$, it can be simply written as

$$u = \frac{1}{L} \sum_{i=1}^L \frac{1 - \phi_{i-1}}{2} \frac{1 + \phi_i}{2} = \frac{1}{L} \sum_{i=1}^L (1 - n_{i-1}) n_i, \quad (49)$$

where $n_i = (1 + \phi_i)/2$ corresponds to the hard-core lattice-gas occupation number. The constraint $\sum_{i=1}^L \phi_i = 0$ translates to $\sum_{i=1}^L n_i = L/2$. Note that here $\langle u \rangle = \langle (1 - n_{i-1}) n_i \rangle$ is proportional to the average current. Knowing the exact steady-state probability distribution [24,25], one can easily find that

$$\langle n_i \rangle = \frac{1}{2}, \quad \langle n_i n_j \rangle_{i \neq j} = \frac{1}{4} \frac{L-2}{L-1}. \quad (50)$$

Thus, the exact finite-size effect for the local minimum density (which is also the average growth rate of the surface [1]) is

$$\langle u \rangle_L = \frac{1}{4} \frac{L}{L-1} = \frac{1}{4} + \frac{1}{4L} + O(L^{-2}), \quad (51)$$

in agreement with the general scaling behavior of $\langle u \rangle_L$ in the EW universality class [Eq. (28)].

B. The massively parallel exponential update model

One of the most challenging problems in parallel computing [26] is the efficient implementation of dynamic Monte Carlo (MC) algorithms for discrete-event simulations on massively parallel architectures. As already mentioned in the Introduction, it has numerous practical applications ranging from magnetic systems (the discrete events are spin-flip attempts) to queueing networks (the discrete events are job arrivals). A parallel architecture by definition contains (usually) a large number of processors, or processing elements (PEs). During the simulation each processor has to tackle only a fraction of the full computing task (e.g., a specific block of spins), and the algorithm has to ensure through synchronization that the underlying dynamics is not altered. In a wide range of models the discrete events are Poisson arrivals. Since this stochastic process is reproductive (the sum of two Poisson processes is also a Poisson process with a different arrival frequency), the Poisson streams can be simulated simultaneously on the subsystems carried by each PE. As a consequence, the simulated time is *local* and *random*, incremented by exponentially distributed random variables on each PE. However, the algorithm has to ensure that causality across the boundaries of the neighboring blocks is not violated. This requires a comparison between the neighboring simulated times, and waiting, if necessary (conservative approach). In the simplest scenario (one site per PE), this means that the only PEs allowed to attempt to update the state of the underlying site and increment their local time are those for which the local simulated time is a *local minimum* of the full simulated time horizon of the system $\{\tau_i\}$, $i = 1, \dots, L$. Here, we consider a chainlike connectivity among the PEs but connectivities of higher degree can be treated as well. Also note that the ‘‘mean-field-like’’ K -random interaction model (each site compares its local simulated time to K randomly chosen other sites) has been investigated by Greenberg *et al.* [28].

One can think of the time horizon as a fluctuating surface with height variable τ_i . Other examples where the update attempts are independent Poisson arrivals include arriving calls in the wireless cellular network of a large metropolitan area [3], or the spin-flip attempts in an Ising ferromagnet. This extremely robust parallel scheme was introduced by Lubachevsky [27], and it is applicable to a wide range of stochastic cellular automata with local dynamics where the discrete events are Poisson arrivals. The local random time increments are, in the language of the associated surface, equivalent to depositing random amounts of ‘‘material’’ (with an exponential distribution) at the local minima of the surface (Fig. 2). This defines a simple surface-growth model which we shall refer to as the massively parallel exponential update (MPEU) model. The main concern about a parallel

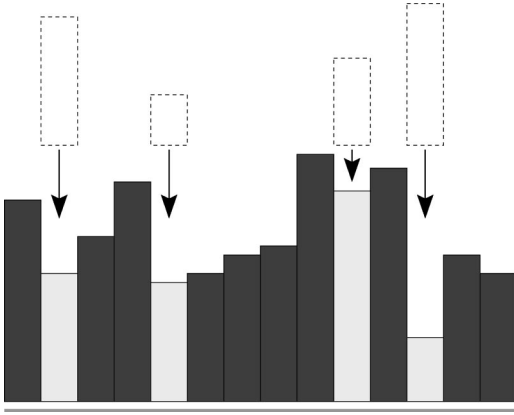


FIG. 2. The MPEU model. The arrows show the local minima, where random amounts of material will be deposited in the next time step.

implementation is its efficiency. Since in the next time step only a fraction of PEs will attempt the update, i.e., those that are in the local minima of the time horizon, while the rest idle, the efficiency is simply the average number of non-idling PEs divided by the total number of PEs (L). This is equivalent to the *average number of minima per unit length*, or the minimum-point density u . The fundamental question of *scalability* arises: will the efficiency of the algorithm go to zero as the number of PEs is increased indefinitely ($L \rightarrow \infty$), or not? If the efficiency has a nonzero lower bound for $L \rightarrow \infty$, the algorithm is called *scalable*, and certainly this is the preferred type of scheme. Can one in principle design such efficient algorithms?

As mentioned in the Introduction, we know of one example that nature provides with an efficient algorithm for a very large number of processing elements: the human brain with its 10^{11} PEs is the largest parallel computer ever built. Although intuition suggests that indeed there are scalable parallel schemes, it has been proved only recently (see Ref. [2] for details), by using the aforementioned analogy with the simple MPEU surface-growth model. While the MPEU model *exactly* mimics the evolution of the simulated time horizon, it can also be considered as a primitive model for ion sputtering of surfaces (etching dynamics): to see this, define a new height variable via $h_i \equiv -\tau_i$, i.e., flip Fig. 2 upside down. This means that, instead of depositing material, we have to take “etch,” and this has to be done at the local *maxima* of the $\{h_i\}$ surface. In sputtering of surfaces by ion bombardment an incoming ion projectile will most likely break off a piece from the *top* of a mound instead of from a valley, very similar to our “reversed” MPEU model. It has been shown that the sputtering process is described by the KPZ equation [16,29]. This qualitative argument is in complete agreement with the extensive MC simulations and coarse-grained approximation of Ref. [2]. The MPEU model is similar to the single-step model in that it also belongs to the KPZ dynamic universality class. In one dimension the macroscopic landscape is governed by the EW Hamiltonian.

The slope variables ϕ_i for MPEU are not independent in the $L \rightarrow \infty$ limit, but short-range correlated. This already guarantees that the steady-state behavior is governed by the EW Hamiltonian, and thus that the density of local minima does not vanish in the thermodynamic limit. Our results con-

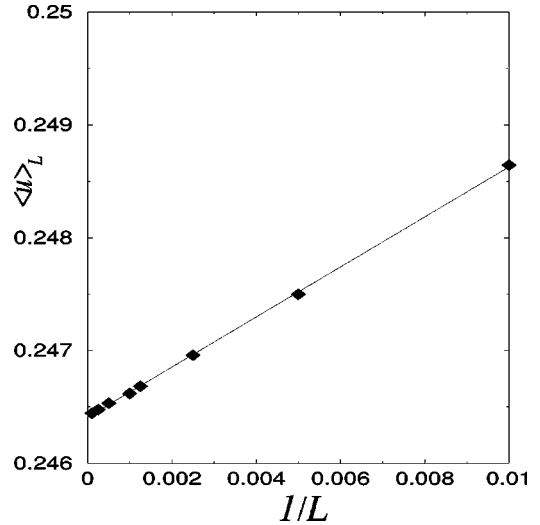


FIG. 3. Density of minima vs $1/L$ for the MPEU model.

firm that the finite-size effects for $\langle u \rangle$ follow Eq. (28):

$$\langle u \rangle_L \simeq \langle u \rangle_\infty + \frac{\text{const}}{L} \quad (52)$$

with $\langle u \rangle_\infty = 0.24641(7)$ (see Fig. 3).

We concluded [2] that the basic algorithm (one site per PE) is scalable for one-dimensional arrays. The same correspondence can be applied to model the performance of the algorithm for higher-dimensional logical PE topologies. While this will involve the typical difficulties of surface-growth modeling, such as an absence of exact results and very long simulation times, it establishes potentially fruitful connections between two traditionally separate research areas.

C. The larger curvature model

In this subsection we briefly present a curvature-driven SOS surface deposition model known in the literature as the larger curvature model, and show a numerical analysis of the density of minima in this model. This model was originally introduced by Kim and Das Sarma [30] and Krug [31] independently, as an atomistic deposition model that fully conforms to the behavior of the continuum fourth-order linear Mullins equation [$\nu=0$, $\kappa>0$ in Eq. (4)]. Note that the discrete analysis we presented in Sec. II is based on the discretization of the continuum equation using the simplest forward Euler differencing scheme. The larger curvature model, however, is a *growth* model where the freshly deposited particles diffuse on the surface according to the rules of the model until they are embedded. Since in all the quantities studied so far the correspondence (on the level of scaling) between the larger curvature model and the Langevin equation is very good, we would expect the dynamic scaling properties of the density of minima for both the model and the equation to be identical.

The larger curvature model has rather simple rules: a freshly deposited atom (let us say at site i) will be incorporated at the nearest-neighbor site that has largest curvature (i.e., $K_i = h_{i+1} + h_{i-1} - 2h_i$ is maximum). If there are more neighbors with the same maximum curvature, then one is

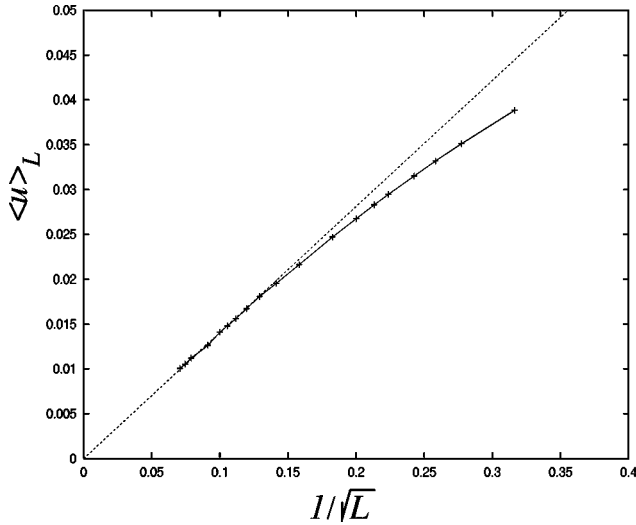


FIG. 4. Density of minima in the steady state for the larger curvature model.

chosen randomly. If the original site (i) is among those with maximum curvature, then the atom is incorporated at i .

Figure 4 shows the scaling of the density of minima $\langle u \rangle_L$ in the steady state vs $1/\sqrt{L}$. According to Eq. (32), for the fourth-order equation on the lattice, the behavior of the density of minima in the steady state scales with system size as $1/\sqrt{L}$. And, indeed, Fig. 4 shows the same behavior for the larger curvature model, as expected. Note that this behavior has already set in at rather small system sizes, about $L = 100$, meaning that the finite-system-size effects are rather small for the larger curvature model. This is a very fortunate property since increasing the system size means decreasing the density of minima, and therefore relative statistical errors will increase.

This can be improved only by better statistics, which, however, quickly becomes a daunting task, since the cross-over time toward the steady state scales with system size as L^4 . As we shall see in Sec. V A, a mathematically rigorous approach to the continuum equation yields the same $1/\sqrt{L}$ behavior. Since the density of minima does decay to zero, an algorithm corresponding to the larger curvature model (or the Mullins equation) would *not* be asymptotically scalable.

Finally, we would like to make a brief note about the observed morphologies in the steady state for the Mullins equation, or the related models. It has been shown previously [32] that in the steady state the morphology typically shows a single large mound (or macroscopic groove). At first sight this may appear as a surprise, since we have shown that the number of minima (or maxima) diverges as \sqrt{L} (the density vanishes as $1/\sqrt{L}$). There is, however, no contradiction, because that refers to a mound that expands throughout the system, i.e., it is a long-wavelength structure, whereas the number of minima measures *all* the minima, and thus it is a short-wavelength characteristic. In the steady state we indeed have a single large, macroscopic groove; however, there are numerous small dips and humps generated by the constant coupling to the noise.

IV. EXTREMAL-POINT DENSITIES ON THE CONTINUUM

Let us consider a continuous and at least two times differentiable function $f: [0, L] \rightarrow \mathbb{R}$. We are interested in count-

ing the total number of extrema of f in the $[0, L]$ interval. The topology of continuous curves in one dimension allows for three possibilities on the nature of a point x_i for which $f'|_{x_i} = 0$, namely, x_i is a local minimum if $f''|_{x_i} > 0$, a local maximum if $f''|_{x_i} < 0$, and degenerate if $f''|_{x_i} = 0$. We call the point x_i a degenerate flat of order k , if $f^{(j)}|_{x_i} = 0$ for $j = 1, 2, \dots, k$ and $f^{(k+1)}|_{x_i} \neq 0$, $k \geq 2$, assuming that the higher-order derivatives $f^{(j)}$ implied exist. The counterlike quantity

$$c(L, [f]) \equiv \frac{1}{L} \int_0^L dx |f''| \delta(f'), \quad (53)$$

where δ is the Dirac delta, gives the number of extremum points per unit length in the interval $[0, L]$, which in the limit of $L \rightarrow 0$ is the extremum-point density of f in the origin. For our purposes L will always be a finite number; however, for the sake of brevity we shall refer to c simply as the density of extrema. Note that counting the extrema of a function f is equivalent to counting the zeros of its derivative f' . The divergence of c for finite L implies the existence of either completely flat regions (infinitely degenerate), or an ‘‘infinitely wrinkled’’ region, such as for the truncated Weierstrass function shown in Fig. 2 (in this latter case the divergence is understood by taking the limit $M \rightarrow \infty$). As already explained in the Introduction, this infinitely wrinkled region does not necessarily imply that the curve is fractal, but if the curve is fractal, then regions of infinite wrinkledness must exist. The divergence or nondivergence of c can be used as an indicator of the existence of such regions (completely flat or infinitely wrinkled).

One can make the following precise statement related to the counter c : if x_i is an extremum point of f of at most finite degeneracy k , and if there exists a small enough ϵ , such that f is analytic in the neighborhood $[x_i - \epsilon, x_i + \epsilon]$, and there are no other extrema in this neighborhood, then

$$I(x_i) \equiv \int_{x_i - \epsilon}^{x_i + \epsilon} dx |f''| \delta(f') = 1, \quad 0 < \epsilon \ll 1, \quad (54)$$

In the following we give a proof of this statement.

Using Taylor-series expansions around x_i , one writes

$$f'(x) = \frac{a_k}{k!} (x - x_i)^k + \frac{a_{k+1}}{(k+1)!} (x - x_i)^{k+1} + \dots, \quad (55)$$

$$f''(x) = \frac{a_k}{(k-1)!} (x - x_i)^{k-1} + \frac{a_{k+1}}{k!} (x - x_i)^k + \dots, \quad (56)$$

where we introduced the shorthand notation $a_j \equiv f^{(j+1)}|_{x_i}$. For the nondegenerate case of $k=1$, Eq. (54) follows from a classical property of the δ function, namely,

$$\delta(g(x)) = \sum_i |g'(x_i)|^{-1} \delta(x - x_i),$$

$$x_i \text{ are simple zeros of } g. \quad (57)$$

Let us now assume that x_i is degenerate of order k ($k \geq 2$). Using the expansions (55) and (56), the variable change $u = x - x_i$, and the well-known property $\delta(ax) = |a|^{-1} \delta(x)$, we obtain

$$I(x_i) = k \int_{-\epsilon}^{\epsilon} du |u|^{k-1} \left| 1 + \sum_{j=1}^{\infty} \frac{(k-1)!}{(k-1+j)!} \frac{a_{k+j}}{a_k} u^j \right| \times \delta \left(|u|^k \left[1 + \sum_{j=1}^{\infty} \frac{k!}{(k+j)!} \frac{a_{k+j}}{a_k} u^j \right] \right). \quad (58)$$

Next we split the integral (58) in two, $\int_{-\epsilon}^{\epsilon} \dots = \int_{-\epsilon}^0 \dots + \int_0^{\epsilon} \dots$, make the variable change $u \rightarrow -u$ in the first one, and then $z = u^k$ in both integrals. The final expression can then be written in the form

$$I(x_i) = \int_{-\epsilon^k}^{\epsilon^k} dz |A(z)| \delta(zB(z)), \quad (59)$$

where

$$A(z) = 1 + \sum_{j=1}^{\infty} \frac{(k-1)!}{(k-1+j)!} \frac{a_{k+j}}{a_k} z^j |z|^{j/k-j}$$

and

$$B(z) = 1 + \sum_{j=1}^{\infty} \frac{k!}{(k+j)!} \frac{a_{k+j}}{a_k} z^j |z|^{j/k-j}. \quad (60)$$

We have $A(0) = B(0) = 1$, and

$$[zB(z)]' = 1 + \sum_{j=1}^{\infty} \frac{k!}{(k+j)!} \frac{a_{k+j}}{a_k} \left(\frac{j}{k} + 1 \right) z^j |z|^{j/k-j} \Rightarrow [zB(z)]'|_{z=0} = 1. \quad (61)$$

(Take the derivatives separately to the right and to the left of $z=0$.) Thus, since $z=0$ is a *simple* zero of $zB(z)$, property (57) can be applied for sufficiently small ϵ :

$$I(x_i) = |A(0)| = 1, \quad (62)$$

proving our assertion. Note that, because of Eq. (54), c counts *all* the nondegenerate and the finitely degenerate points as well, giving equal weight of unity to each. Can we count the nondegenerate extrema separately? The answer is affirmative, if one considers instead of Eq. (53) the following quantity:

$$c_q(L, [f]) \equiv \frac{1}{L} \int_0^L dx |f''|^{q+1} \delta(f'), \quad q > 0. \quad (63)$$

Performing the same steps as above we obtain for a degenerate point

$$I_q(x_i) \equiv \int_{x_i-\epsilon}^{x_i+\epsilon} dx |f''|^{q+1} \delta(f') = \left(\frac{|a_k|}{(k-1)!} \right)^q \int_{-\epsilon^k}^{\epsilon^k} dz |z|^{q(1-1/k)} |A(z)|^{q+1} \delta(zB(z)). \quad (64)$$

Since $k \geq 2$, $q(1-1/k) \geq \frac{1}{2}q > 0$, i.e.,

$$I_q(x_i) = 0 \quad \text{for } x_i \text{ degenerate.} \quad (65)$$

This means that $q > 0$ eliminates the degenerate points from the count. To nondegenerate points ($k=1$) Eq. (63) gives the weight of

$$I_q(x_i) = |a_1|^q = |f''|_{x_i}^q \quad \text{for } x_i \text{ nondegenerate.} \quad (66)$$

In other words,

$$c_q(L, [f]) = \frac{1}{L} \sum_i |K(x_i)|^q, \quad q > 0, \quad x_i \text{ nondegenerate extrema of } f, \quad (67)$$

where $K(x) = f''$ is the *curvature* of f at x . The limit $q \rightarrow 0^+$ in Eq. (67) gives the extremum-point density $\bar{c}(L, [f])$ of f of nondegenerate extrema:

$$\bar{c}(L, [f]) = \lim_{q \rightarrow 0^+} c_q(L, [f]) = \lim_{q \rightarrow 0^+} \frac{1}{L} \int_0^L dx |f''|^{q+1} \delta(f'). \quad (68)$$

It is important to note that taking the $q \rightarrow 0^+$ limit in Eq. (67) is *not equivalent* to taking $q=0$ in Eq. (63), i.e., the limit and the integral on the right-hand side of Eq. (68) are not interchangeable. The difference is the set of degenerate points.

Until now, we did not make any distinction between maxima and minima. In a natural way, we expect that the quantity

$$u(L, [f]) \equiv \frac{1}{L} \int_0^L dx f'' \delta(f') \theta(f''), \quad (69)$$

where $\theta(x)$ is the Heaviside step function, will give the density of minima (due to the step function, here we can drop the absolute values). However, performing a similar derivation to the one above, one concludes that Eq. (69) is somewhat ill defined, in the sense that the weight given to degenerate points depends on the definition of the step function at the origin [however, $u(L, [f])$ is bounded]. Introducing a *q regulator* as above, the weight of degenerate points is pulled down to zero:

$$u_q(L, [f]) \equiv \frac{1}{L} \int_0^L dx [f'']^{q+1} \delta(f') \theta(f''), \quad q > 0, \quad (70)$$

and

$$u_q(L, [f]) = \frac{1}{L} \sum_i [K(x_i)]^q, \quad q > 0, \quad x_i \text{ nondegenerate minima of } f. \quad (71)$$

Note that in the equation above the absolute values are not needed, since we are summing over the curvatures of all local *minima*. The density $\bar{u}(L,[f])$ of nondegenerate minima of f is obtained after taking the limit $q \rightarrow 0^+$:

$$\bar{u}(L,[f]) = \lim_{q \rightarrow 0^+} u_q(L,[f]), \quad (72)$$

and the limit is not interchangeable with the integral in Eq. (70). To obtain densities for maxima, one only has to replace the argument f'' of the Heaviside function with $-f''$.

A. Stochastic extremal-point densities

We are interested in exploring the previously introduced quantities for a stochastic function subject to time evolution $h(x,t)$. This function may, for example, be the solution to a Langevin equation. We define the two basic quantities in the same way as before, except that now one performs a stochastic average over the noise, as well:

$$C_q(L,t) = \left\langle \frac{1}{L} \int_0^L dx \left| \frac{\partial^2 h}{\partial x^2} \right|^{q+1} \delta \left(\frac{\partial h}{\partial x} \right) \right\rangle$$

and

$$U_q(L,t) = \left\langle \frac{1}{L} \int_0^L dx \left[\frac{\partial^2 h}{\partial x^2} \right]^{q+1} \delta \left(\frac{\partial h}{\partial x} \right) \theta \left(\frac{\partial^2 h}{\partial x^2} \right) \right\rangle. \quad (73)$$

For systems preserving translational invariance, the stochastic average of the integrand becomes x independent, and the integrals can be dropped:

$$C_q(L,t) = \left\langle \left| \frac{\partial^2 h}{\partial x^2} \right|^{q+1} \delta \left(\frac{\partial h}{\partial x} \right) \right\rangle, \quad (74)$$

$$U_q(L,t) = \left\langle \left(\frac{\partial^2 h}{\partial x^2} \right)^{q+1} \delta \left(\frac{\partial h}{\partial x} \right) \theta \left(\frac{\partial^2 h}{\partial x^2} \right) \right\rangle. \quad (75)$$

According to Eqs. (67) and (71), $C_q(L,t)$ and $U_q(L,t)$ can be thought of as time-dependent ‘‘partition functions’’ for the nondegenerate extremal-point densities of the underlying stochastic process, with q playing the role of ‘‘inverse temperature’’:

$$C_q(L,t) = \left\langle \frac{1}{L} \sum_i |K(x_i)|^q \right\rangle, \quad (76)$$

$q > 0, \quad x_i \text{ nondegenerate } \textit{extrema},$

$$U_q(L,t) = \left\langle \frac{1}{L} \sum_i [K(x_i)]^q \right\rangle, \quad (77)$$

$q > 0, \quad x_i \text{ nondegenerate } \textit{minima}.$

It is important to mention that in the above equations the average $\langle \dots \rangle$ and the summation are *not* interchangeable: particular realizations of h have particular sets of minima.

Two values for q are of special interest: $q \rightarrow 0^+$ and $q = 1$. In the first case we obtain the stochastic average of the density of nondegenerate extrema and minima:

$$\bar{C}(L,t) = \lim_{q \rightarrow 0^+} C_q(L,t) \quad \text{and} \quad \bar{U}(L,t) = \lim_{q \rightarrow 0^+} U_q(L,t), \quad (78)$$

and in the second case we obtain the stochastic average of the mean curvature at extrema and minima:

$$\bar{K}_{\text{ext}}(L,t) = \frac{C_1(L,t)}{\bar{C}(L,t)} \quad \text{and} \quad \bar{K}_{\text{min}}(L,t) = \frac{U_1(L,t)}{\bar{U}(L,t)} \quad (79)$$

(we need to normalize with the number of extrema or minima per unit length to get the curvature per extremum or minimum).

In the following we explore the quantities (74)–(79) for a large class of linear Langevin equations. To simplify the calculations, we will assume that q is a positive integer. Then we will attempt analytic continuation on the final result as a function of q . In the calculations we will make extensive use of the standard integral representations of the δ and step functions:

$$\delta(y) = \int_{-\infty}^{\infty} \frac{dz}{2\pi} e^{izy} = \sum_{n=0}^{\infty} \int_{-\infty}^{\infty} \frac{dz}{2\pi} \frac{(iz)^n}{n!} y^n, \quad (80)$$

$$\begin{aligned} \theta(y) &= \lim_{\epsilon \rightarrow 0^+} \int_{-\infty}^{\infty} \frac{dz}{2\pi} \frac{e^{izy}}{\epsilon + iz} \\ &= \lim_{\epsilon \rightarrow 0^+} \sum_{n=0}^{\infty} \int_{-\infty}^{\infty} \frac{dz}{2\pi} \frac{1}{\epsilon + iz} \frac{(iz)^n}{n!} y^n. \end{aligned} \quad (81)$$

If q is a positive odd integer, we may drop the absolute value signs in Eq. (74). In general, the absolute values make the calculation of stochastic averages very difficult. We can get around this problem by employing the following identity:

$$|y|^n = y^n \{ (-1)^n + \theta(y) [1 - (-1)^n] \}. \quad (82)$$

This brings Eq. (74) to

$$C_q(L,t) = [1 - (-1)^{q+1}] U_q(L,t) + (-1)^{q+1} B_q(L,t), \quad (83)$$

where

$$\begin{aligned} B_q(L,t) &= \left\langle \frac{1}{L} \int_0^L dx \left(\frac{\partial^2 h}{\partial x^2} \right)^{q+1} \delta \left(\frac{\partial h}{\partial x} \right) \right\rangle \\ &= \left\langle \left(\frac{\partial^2 h}{\partial x^2} \right)^{q+1} \delta \left(\frac{\partial h}{\partial x} \right) \right\rangle. \end{aligned} \quad (84)$$

Obviously, for q an odd integer, $B_q = C_q$. For q even, B_q is an interesting quantity by itself. In this case the weight of an extremum x_i is $\text{sgn}[K(x_i)] |K(x_i)|^q$. If the analytic continuation can be performed, then the $q \rightarrow 0^+$ limit will tell us if there are more nondegenerate maxima than minima (or otherwise) on average. Using the integral representations (80) and (81) we find

$$B_q(L,t) = \sum_{n=0}^{\infty} \int_{-\infty}^{\infty} \frac{dz}{2\pi} \frac{(iz)^n}{n!} \left\langle \left(\frac{\partial^2 h}{\partial x^2} \right)^{q+1} \left(\frac{\partial h}{\partial x} \right)^n \right\rangle, \quad (85)$$

$$\begin{aligned}
U_q(L,t) &= \lim_{\epsilon \rightarrow 0^+} \sum_{n_1=0}^{\infty} \sum_{n_2=0}^{\infty} \int_{-\infty}^{\infty} \frac{dz_1}{2\pi} \frac{(iz_1)^{n_1}}{n_1!} \\
&\times \int_{-\infty}^{\infty} \frac{dz_2}{2\pi} \frac{(iz_2)^{n_2}}{n_2!} \frac{1}{\epsilon + iz_2} \\
&\times \left\langle \left(\frac{\partial^2 h}{\partial x^2} \right)^{n_2+q+1} \left(\frac{\partial h}{\partial x} \right)^{n_1} \right\rangle. \quad (86)
\end{aligned}$$

V. EXTREMAL-POINT DENSITIES OF LINEAR STOCHASTIC EVOLUTION EQUATIONS

Next we calculate the densities (85) and (86) for the following type of linear stochastic equations

$$\frac{\partial h}{\partial t} = -\nu(-\nabla^2)^{z/2}h + \eta(x,t), \quad \nu, D, z > 0, \quad x \in [0, L], \quad (87)$$

with initial condition $h(x,0)=0$, for all $x \in [0, L]$. Here, η is a white noise term drawn from a Gaussian distribution with zero mean $\langle \eta(x,t) \rangle = 0$, and covariance

$$\langle \eta(x,t) \eta(x',t') \rangle = 2D \delta(x-x') \delta(t-t'). \quad (88)$$

We also performed our calculations with other noise types, such as volume conserving and long-range correlated ones; however, the details are lengthy to be included in the present paper and will be the subject of a future publication. As boundary condition we choose periodic boundaries:

$$h(x+nL,t) = h(x,t), \quad \eta(x+nL,t) = \eta(x,t) \quad \text{for all } n \in \mathbb{Z}. \quad (89)$$

The general solution to Eq. (87) is obtained simply with the help of Fourier series [17]. The Fourier series and its coefficients for a function f defined on $[0, L]$ is

$$f(x) = \sum_k \tilde{f}(k) e^{ikx}, \quad \tilde{f}(k) = \frac{1}{L} \int_{-L}^L dx f(x) e^{-ikx}, \quad (90)$$

where $k = (2\pi/L)n$, $n = \dots, -2, -1, 0, 1, 2, \dots$. The Fourier coefficients of the general solution to Eq. (87) are

$$\tilde{h}(k,t) = \int_0^t dt' e^{-\nu|k|^z(t-t')} \tilde{\eta}(k,t'). \quad (91)$$

The correlations of the noise in momentum space are

$$\langle \tilde{\eta}(k,t) \tilde{\eta}(k',t') \rangle = \frac{2D}{L} \delta_{k,-k'} \delta(t-t'). \quad (92)$$

Due to the Gaussian character of the noise, the two-point correlation of the solution (91) is also δ correlated, and it completely characterizes the statistical properties of the stochastic dynamics (87). It is given by

$$\langle \tilde{h}(k,t) \tilde{h}(k',t') \rangle = S(k,t) \delta_{k,-k'}, \quad (93)$$

where $S(k,t)$ is the structure factor,

$$S(k,t) = \frac{D}{\nu L |k|^z} (1 - e^{-2\nu|k|^z t}). \quad (94)$$

Equation (87) has been analyzed in great detail by a number of authors (see Ref. [17] for a review). It was shown that there exists an upper critical dimension $d_c = z$ for Eq. (87) which separates the rough regime with $d < z$ from the non-roughening regime $d > z$. In one dimension, the rough regime corresponds to the condition $z > 1$, which we shall assume from now on, since this is where the interesting physics lies.

Next, we evaluate the quantities (74)–(79) by directly calculating the expressions in Eqs. (85) and (86). This amounts to computing averages of the type

$$\mathcal{Q}_{N,M} = \left\langle \left(\frac{\partial^2 h}{\partial x^2} \right)^N \left(\frac{\partial h}{\partial x} \right)^M \right\rangle. \quad (95)$$

Expressing h with its Fourier series according to Eq. (90), we write

$$\begin{aligned}
\left(\frac{\partial h}{\partial x} \right)^M &= i^M \sum_{k_1} \dots \sum_{k_M} k_1 \dots k_M \tilde{h}(k_1, t) \dots \tilde{h}(k_M, t) \\
&\times e^{i(k_1 + \dots + k_M)x}, \quad (96)
\end{aligned}$$

$$\begin{aligned}
\left(\frac{\partial^2 h}{\partial x^2} \right)^N &= (-1)^N \sum_{k'_1} \dots \sum_{k'_N} k'^2_1 \dots k'^2_N \tilde{h}(k'_1, t) \dots \tilde{h}(k'_N, t) \\
&\times e^{i(k'_1 + \dots + k'_N)x}, \quad (97)
\end{aligned}$$

which then is inserted in Eq. (95). Thus one needs to calculate averages in Fourier space of the type $\langle \tilde{h}(k_1, t) \dots \tilde{h}(k_M, t) \tilde{h}(k'_1, t) \dots \tilde{h}(k'_N, t) \rangle$. According to Eq. (93) \tilde{h} is anti- δ -correlated; therefore these averages can be performed in the standard way [33] by taking all the possible pairings of indices and employing Eq. (93). In our case there are three types of pairings: $\{k_j, k_l\}$, $\{k_j, k'_l\}$, and $\{k'_j, k'_l\}$. Let us pick a ‘‘mixed’’ pair $\{k_j, k'_l\}$ containing a primed and a nonprimed index. The corresponding contribution in $\mathcal{Q}_{N,M}$ will be

$$\sum_{k_j} \sum_{k'_l} k_j k'^2_l S(k'_l, t) e^{i(k_j + k'_l)x} \delta_{k_j, -k'_l}. \quad (98)$$

Since the structure factor $S(k,t)$ is an even function in k , Eq. (98) becomes $\sum_{k_j} k_j^3 S(k_j, t) = 0$, because the summand is an odd function of k_j and the summation is symmetric around zero. Thus, it is enough to consider nonmixed index pairs only. This means that $\mathcal{Q}_{N,M}$ decouples into

$$\mathcal{Q}_{N,M} = \left\langle \left(\frac{\partial^2 h}{\partial x^2} \right)^N \right\rangle \left\langle \left(\frac{\partial h}{\partial x} \right)^M \right\rangle. \quad (99)$$

The averages are calculated easily, and we find

$$\left\langle \left(\frac{\partial h}{\partial x} \right)^M \right\rangle = \begin{cases} (M-1)!! [\phi_2(L,t)]^{M/2} & \text{for } M \text{ even} \\ 0 & \text{for } M \text{ odd,} \end{cases} \quad (100)$$

and

$$\left\langle \left(\frac{\partial^2 h}{\partial x^2} \right)^N \right\rangle = \begin{cases} (N-1)!! [\phi_4(L,t)]^{N/2} & \text{for } N \text{ even} \\ 0 & \text{for } N \text{ odd,} \end{cases} \quad (101)$$

where

$$\phi_m(L,t) \equiv \sum_k |k|^m S(k,t). \quad (102)$$

Employing Eqs. (100) and (101) in Eq. (85), it follows that if q is an even integer, $q=2s$, $s=1,2,\dots$, then

$$B_{2s}(t) = 0, \quad s=1,2,\dots, \quad (103)$$

whereas for q an odd integer, $q=2s-1$, $s=1,2,\dots$,

$$B_{2s-1}(t) = C_{2s-1}(t) = \frac{2^{s-1/2}}{\pi} \Gamma\left(s + \frac{1}{2}\right) \frac{[\phi_4(L,t)]^s}{\sqrt{\phi_2(L,t)}}, \quad s=1,2,\dots, \quad (104)$$

where we used the identity $2^p(2p-1)!!/(2p)! = 1/p!$ and performed the Gaussian integral.

The calculation of U_q is a bit trickier. The sum over n_1 in Eq. (86) is easy and leads to the Gaussian $e^{-\phi_2(L,t)z_1^2/2}$. However, the sum over n_2 is more involved. Let us make the temporary notation for the sum over n_2 :

$$R_q = \sum_{n_2=0}^{\infty} \frac{(iz_2)^{n_2}}{n_2!} (2r-1)!! [\phi_4(L,t)]^r, \quad n_2 + q + 1 = 2r. \quad (105)$$

We have to distinguish two cases according to the parity of q .

(1) q is odd, $q=2s-1$, $s=1,2,\dots$. In this case R_q becomes

$$R_{2s-1} = \sum_{r=s}^{\infty} \frac{(iz_2)^{2(r-s)}}{[2(r-s)]!} \frac{(2r)!}{r!} \left(\frac{1}{2} \phi_4(L,t) \right)^r = (z_2)^{-2s} (-1)^s \left[\frac{\partial^{2s}}{\partial x^{2s}} (e^{-\phi_4(L,t)z_2^2 x^2/2}) \right]_{x=1}. \quad (106)$$

The Hermite polynomials are defined via the Rodrigues formula as

$$H_n(x) = (-1)^n e^{x^2} \frac{d^n}{dx^n} (e^{-x^2}). \quad (107)$$

Using this, we can express R_{2s-1} with the help of Hermite polynomials:

$$R_{2s-1} = (-1)^s \left(\frac{1}{2} \phi_4(L,t) \right)^s H_{2s} \left(\sqrt{\frac{1}{2} \phi_4(L,t)} z_2 \right) \times e^{-\phi_4(L,t)z_2^2 x^2/2}. \quad (108)$$

(2) q is even, $q=2s$, $s=1,2,\dots$. The calculations are analogous to the odd case:

$$R_{2s} = \sum_{r=s+1}^{\infty} \frac{(iz_2)^{2(r-s)-1}}{[2(r-s)-1]!} \frac{(2r)!}{r!} \left(\frac{1}{2} \phi_4(L,t) \right)^r = (iz_2)^{-2s-1} \left[\frac{\partial^{2s+1}}{\partial x^{2s+1}} (e^{-\phi_4(L,t)z_2^2 x^2/2}) \right]_{x=1} \quad (109)$$

or, via Hermite polynomials,

$$R_{2s} = i(-1)^s \left(\frac{1}{2} \phi_4(L,t) \right)^{s+1/2} H_{2s+1} \left(\sqrt{\frac{1}{2} \phi_4(L,t)} z_2 \right) \times e^{-\phi_4(L,t)z_2^2 x^2/2}. \quad (110)$$

In order to obtain U_q we have to do the integral over z_2 in Eq. (86). This can be obtained after using the formula

$$\int_{-\infty}^{\infty} dx (x \pm ic)^\nu H_n(x) e^{-x^2} = 2^{n-1-\nu} \sqrt{\pi} \frac{\Gamma((n-\nu)/2)}{\Gamma(-\nu)} \times e^{\pm(i\pi/2)(\nu+n)}, \quad c \rightarrow 0^+. \quad (111)$$

Finally, the densities for the minima read as

$$U_{2s}(t) = \frac{2^{s-1}}{\pi} \Gamma(s+1) \frac{[\phi_4(L,t)]^{s+1/2}}{\sqrt{\phi_2(L,t)}}, \quad (112)$$

$$U_{2s-1}(t) = \frac{2^{s-3/2}}{\pi} \Gamma\left(s + \frac{1}{2}\right) \frac{[\phi_4(L,t)]^s}{\sqrt{\phi_2(L,t)}}. \quad (113)$$

Formulas (103), (104), (112), and (113) combined with Eq. (83) can be condensed very simply, and we obtain the general result as

$$U_q(L,t) = \frac{2^{q/2-1}}{\pi} \Gamma\left(\frac{q}{2} + 1\right) \frac{[\phi_4(L,t)]^{(q+1)/2}}{\sqrt{\phi_2(L,t)}}, \quad (114)$$

$$C_q(L,t) = 2U_q(L,t). \quad (115)$$

Equations (114) and (115) together with Eq. (113) fully solve the problem for the density of nondegenerate extrema. Equation (115) is an expected result in one dimension, because Eq. (87) preserves the up-down symmetry. The density of nondegenerate minima is

$$\bar{U}(L,t) = \lim_{q \rightarrow 0^+} U_q(L,t) = \frac{1}{2\pi} \sqrt{\frac{\phi_4(L,t)}{\phi_2(L,t)}}, \quad (116)$$

and the stochastic average of the mean curvature at a minimum point is

$$\bar{K}(L,t) = \frac{U_1(L,t)}{\bar{U}(L,t)} = \sqrt{\frac{\pi}{2}} \sqrt{\phi_4(L,t)}, \quad (117)$$

i.e., the average curvature at a minimum is proportional to the square root of the fourth moment of the structure factor. In the following section we exploit the physical information behind the above expressions for the stochastic process (87). At some parameter values, a few of, or all, the quantities

above may diverge. In this case we introduce a microscopic lattice cutoff $0 < a \ll 1$, and analyze the limit $a \rightarrow 0^+$ in the final formulas. This in fact corresponds to placing the whole problem on a lattice with lattice constant a . It has been shown in Ref. [17] that for the class of equations (87) there are three important length scales that govern the statistical behavior of the interface h : the lattice constant a , the system size L , and the *dynamical correlation length* ξ defined by

$$\xi(t) \equiv (2\nu t)^{1/z}. \quad (118)$$

According to Eqs. (102) and (94) the function $\phi_m(L, t)$ becomes

$$\phi_m(L, t) = \frac{2D}{\nu L} \sum_{n=0}^{\infty} \left(\frac{2\pi n}{L} \right)^{m-z} (1 - e^{-(\xi 2\pi n/L)^z}), \quad m=2,4. \quad (119)$$

The $n=0$ term can be dropped from the sum above, because it is zero even for $m < z$ (expand the exponential and then take $n=0$). However, the whole sum may diverge depending on m and z . In order to handle all the cases, including the divergent ones, we introduce the microscopic lattice cutoff a , $0 < a \ll 1$, and then analyze the limit $a \rightarrow 0^+$ in the final expressions. Appropriately, Eq. (119) becomes

$$\phi_m(L, t) = \frac{2D}{\nu L} \sum_{n=1}^{L/2a} \left(\frac{2\pi n}{L} \right)^{m-z} (1 - e^{-(\xi 2\pi n/L)^z}), \quad m=2,4. \quad (120)$$

A. Steady-state regime

Putting $\xi = \infty$ in Eq. (120), ϕ_m takes a simpler form:

$$\phi_m(L, \infty) = \frac{2D}{\nu L} \left(\frac{2\pi}{L} \right)^{m-z} \sum_{n=1}^{L/2a} n^{m-z}, \quad m=2,4. \quad (121)$$

As $a \rightarrow 0^+$, ϕ_m becomes proportional to the Riemann's ζ function, $\zeta(z-m)$. For $z-m > 1$, ϕ_m is convergent, otherwise it is divergent. In the divergent case we quote the following results:

$$\sum_{n=1}^N n^s = \ln N + \mathcal{C} + O(1/N) \quad \text{if } s = -1 \quad (122)$$

where \mathcal{C} is the Euler constant, and

$$\sum_{n=1}^N n^s = \frac{N^{s+1}}{s+1} [1 + O(1/N)] \quad \text{if } s > -1, \quad (123)$$

which we will use to derive the leading behavior of the extremal point densities when $L/a \rightarrow \infty$. From Eqs. (121), (114), (116), and (117) it follows that

$$U_q(L, \infty) = \Gamma\left(\frac{q}{2} + 1\right) \left(\frac{2D}{\pi\nu}\right)^{q/2} (2\pi)^{(q/2)(5-z)} L^{-1-(q/2)(5-z)} \times \left[\sum_{n=1}^{L/2a} n^{4-z} \right]^{(q+1)/2} \left[\sum_{n=1}^{L/2a} n^{2-z} \right]^{-1/2}, \quad (124)$$

$$\bar{U}(L, \infty) = \frac{1}{L} \sqrt{\sum_{n=1}^{L/2a} n^{4-z} \left(\sum_{n=1}^{L/2a} n^{2-z} \right)^{-1}}, \quad (125)$$

and

$$\bar{K}(L, \infty) = \sqrt{\frac{D}{2} (2\pi)^{5-z} L^{z-5} \sum_{n=1}^{L/2a} n^{4-z}}. \quad (126)$$

The convergence (divergence) properties of the sums in Eqs. (124)–(126) for $a \rightarrow 0^+$ generate two critical values for z , namely, $z=3$ and $z=5$. In the three regions separated by these values we obtain *qualitatively* different behaviors for the extremal-point densities.

(i) $z > 5$. All quantities are convergent as $a \rightarrow 0^+$. We have

$$U_q(L, \infty) = \Gamma\left(\frac{q}{2} + 1\right) \left(\frac{2D}{\pi\nu}\right)^{q/2} (2\pi)^{(q/2)(5-z)} \times \frac{[\xi(z-4)]^{(q+1)/2}}{[\xi(z-2)]^{1/2}} L^{-1+(q/2)(z-5)}, \quad (127)$$

$$\bar{U}(L, \infty) = \frac{1}{L} \sqrt{\frac{\xi(z-4)}{\xi(z-2)}}, \quad (128)$$

$$\bar{K}(L, \infty) = (2\pi)^{(5-z)/2} \sqrt{\frac{D}{2\nu} \xi(z-4) L^{(z-5)/2}}. \quad (129)$$

Equation (128) shows that there is a finite number of minima $[\sqrt{\xi(z-4)/\xi(z-2)}]$ in the steady state, independently of the system size L . $[\bar{U}(L, \infty)]$ is the number of minima per unit length, and $L\bar{U}(L, \infty)$ is the number of minima on the substrate of size L . The mean curvature $\bar{K}(L, \infty)$ diverges with system size as $L^{(z-5)/2}$. This is consistent with the fact that the system size grows as L , the width grows as $L^{(z-1)/2}$, i.e., faster than L , and thus the peaks and minima should become sleeker and sharper as $L \rightarrow \infty$, expecting diverging curvatures at minima and maxima. However, this is not always true, since the sleekness of the humps and mounds does not necessarily imply large curvatures at minima and maxima if the *shapes* of the humps also change as L changes, i.e., if there is lack of *self-affinity*. The existence of $z=5$ as a critical value is a nontrivial result of the presented analysis.

(ii) $z=5$. According to Eq. (122), $\phi_4(L, \infty)$ diverges logarithmically as $a \rightarrow 0^+$. One obtains

$$U_q(\infty) \approx \Gamma\left(\frac{q}{2} + 1\right) \left(\frac{2D}{\pi\nu}\right)^{q/2} \frac{1}{\sqrt{\xi(3)}} \frac{1}{L} \left(\ln \frac{L}{2a} + \mathcal{C} \right)^{(q+1)/2}, \quad (130)$$

$$\bar{U}(L, \infty) = \frac{1}{\sqrt{\xi(3)}} \frac{1}{L} \sqrt{\ln \frac{L}{2a} + \mathcal{C}}, \quad (131)$$

$$\bar{K}(L, \infty) = \sqrt{\frac{D}{2\nu} \left(\ln \frac{L}{2a} + \mathcal{C} \right)}. \quad (132)$$

Equation (131) shows that, although the density of minima vanishes, the number of minima is no longer a constant but *diverges* logarithmically with system size L . The mean curvature still diverges, but logarithmically, when compared to the power-law divergence of Eq. (129).

For the mean curvature $\bar{K}(\infty)$ in Eq. (126) $z=5$ is the only critical value, since it only depends on ϕ_4 . For $z<5$, using Eq. (123) we arrive at the result that the mean curvature at a minimum point approaches an L -independent constant for $L/a \rightarrow \infty$, with corrections on the order of a/L :

$$\bar{K}(L, \infty) \approx \left(\frac{\pi}{a}\right)^{(5-z)/2} \sqrt{\frac{D}{2\nu(5-z)}}, \quad z < 5. \quad (133)$$

We arrived at the same conclusion in Sec. IID when we studied the steady state of the discretized version of the continuum equation. Coincidentally, for $z=4$ the two constant values from Eqs. (133) and (47) are identical [$a=1$ by definition in Eq. (47)].

(iii) $3 < z < 5$. In this case $\phi_4(L, \infty) \rightarrow \infty$ and $\phi_2(L, \infty) < \infty$ as $a \rightarrow 0^+$,

$$U_q(L, \infty) \approx \Gamma\left(\frac{q}{2} + 1\right) \left(\frac{2D}{\nu\pi}\right)^{q/2} \left(\frac{\pi}{a}\right)^{(q/2)(5-z)} \left(\frac{1}{2a}\right)^{(5-z)/2} \\ \times \frac{L^{-(z-3)/2}}{(5-z)^{(q+1)/2} \sqrt{\xi(z-2)}}, \quad (134)$$

and

$$\bar{U}(L, \infty) \approx \left(\frac{1}{2a}\right)^{(5-z)/2} \frac{L^{-(z-3)/2}}{\sqrt{(5-z)\xi(z-2)}}, \quad (135)$$

and the mean curvature is just given by Eq. (133).

Comparing Eqs. (127), (130), and (134) we can make an interesting observation: while for $z \geq 5$ the dependence on the system size L is coupled to the ‘‘inverse temperature’’ q , for $3 < z < 5$ the dependence on L *decouples* from q , i.e., it becomes independent of the inverse temperature. Equation (135) shows that the density of minima vanishes with system size as a power law with an exponent $(z-3)/2$, but the *number* of minima diverges as a power law with an exponent of $(5-z)/2$.

(iv) $z=3$. In this case $\phi_4(L, \infty) \rightarrow \infty$ and $\phi_2(L, \infty) \rightarrow \infty$ logarithmically as $a \rightarrow 0^+$. One obtains

$$U_q(L, \infty) \approx \frac{1}{2\sqrt{2a}} \Gamma\left(\frac{q}{2} + 1\right) \left(\frac{\pi D}{\nu a^2}\right)^{q/2} \frac{1}{\sqrt{\ln(L/2a) + C}}, \quad (136)$$

and

$$\bar{U}(L, \infty) \approx \frac{1}{2\sqrt{2a}} \frac{1}{\sqrt{\ln(L/2a) + C}}, \quad (137)$$

with a logarithmically vanishing density of minima, and the dependence on the system size in Eq. (136) is not coupled to q .

(v) $1 < z < 3$. Now both ϕ_4 and ϕ_2 diverge as $a \rightarrow 0^+$. Employing Eq. (123) yields

$$U_q(L, \infty) \approx \frac{1}{2a} \Gamma\left(\frac{q}{2} + 1\right) \left(\frac{2D}{\pi\nu}\right)^{q/2} \left(\frac{\pi}{a}\right)^{(q/2)(5-z)} \\ \times \frac{\sqrt{3-z}}{(5-z)^{(q+1)/2}} \quad (138)$$

and

$$\bar{U}(L, \infty) \approx \frac{1}{2a} \sqrt{\frac{3-z}{5-z}}. \quad (139)$$

Note that to leading order both $U_q(L, \infty)$ and the density of minima $\bar{U}(L, \infty)$ become system-size independent. The system-size dependence comes in as *corrections* on the order of a/L and higher. The fact that the efficiency of the massively parallel algorithm presented in Sec. IIIB is not vanishing is due precisely to the above phenomenon: the fluctuations of the time horizon in the steady state belong to the $z=2$ class (Edwards-Wilkinson universality), and according to the results under (iv) the density of minima (or the efficiency of the parallel algorithm) converges to a nonzero constant, as $L \rightarrow \infty$, ensuring the scalability of the algorithm. An algorithm that would map into a $z \geq 3$ class would have a vanishing efficiency with increasing number of processing elements. In particular, for $z=2$, one obtains from Eq. (139) $\bar{U}(L, \infty) \approx (a2\sqrt{3})^{-1} = 0.2886 \dots / a$. Note that the utilization we obtained is somewhat different from in the discrete case, which was approximately $1/4$. This is due to the fact that this number is nonuniversal and it may show differences depending on the discretization scheme used. However, it *cannot* be zero.

Another important conclusion can be drawn from the final results listed above: at and below $z=5$, all the quantities *diverge* when $a \rightarrow 0^+$, and L is fixed. This means that the higher the resolution, the more details we find in the morphology, just as for an infinitely wrinkled or fractal-like surface. We call this transition across $z=5$ a ‘‘wrinkle’’ transition. As shown in the Introduction, wrinkledness can assume two phases depending on whether the curve is a fractal or not and the transition between these two phases may be conceived as a phase transition. However, one may be able to scale the system size L with a such that the quantities calculated will not diverge in this limit. This is possible only in the regime $3 < z < 5$, when we impose

$$L^{z-3} a^{(q+1)(5-z)} = \text{const.} \quad (140)$$

This shows that the rescaling cannot be done for all inverse temperatures q at the same time. In particular, for the density of minima and $z=4$, $La = \text{const.}$

B. Scaling regime

The full temporal behavior of the extremal-point densities can be obtained after employing the Poisson summation formulas (B4) from Appendix B in Eq. (120). Due to lack of space, we will only present the results, leaving the presentation of the details of the derivation to a forthcoming publication. It is important to note that the scaling properties of the dynamics are determined by the dimensionless *ratios* L/ξ and ξ/a . The scaling regime is defined by $a \ll \xi \ll L$.

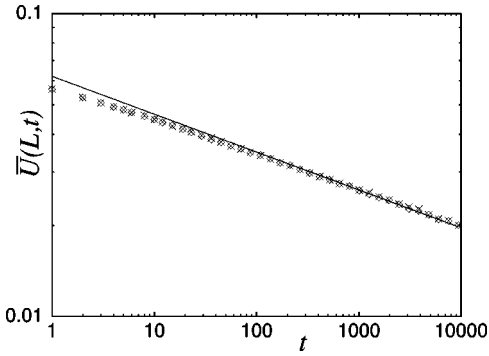


FIG. 5. Density of minima for the larger curvature model as a function of time (the number of deposited layers), for two system sizes, $L=100$ (diamonds) and $L=120$ (crosses). The straight line corresponds to the behavior $t^{-1/8}$.

Just as in the case of steady state, one has to distinguish five situations depending on the values of z , with respect to the critical values 3 and 5.

(i) $z > 5$. The time behavior is a clean power law: $U_q(L,t)$ decays as $\sim t^{-[2+q(z-5)]/2z}$, $\bar{U}(L,t) \sim t^{-1/z}$, and $\bar{K}(L,t)$ diverges as $\sim t^{(z-5)/2z}$, for $L/\xi \gg 1$.

(ii) $z = 5$. In this case the leading temporal behavior has a logarithmic component due to the borderline situation: $U_q(L,t)$ decays as $\sim t^{-1/5}(\ln t)^{(q+1)/2}$, $\bar{U}(L,t) \sim t^{-1/5}(\ln t)^{1/2}$, and $\bar{K}(L,t)$ diverges as $\sim (\ln t)^{1/2}$.

(iii) $3 < z < 5$. Below $z = 5$ the leading time dependence of the partition function $U_q(L,t)$ becomes *independent* of the inverse temperature q , and it presents a clean power-law decay $\sim t^{-(z-3)/2z}$ which is the same also for $\bar{U}(L,t)$. In particular, for $z = 4$ this means a $t^{-1/8}$ decay, which is very well satisfied by the larger curvature model from Sec. III C (see Fig. 5).

Our final expressions also show that the leading term is system-size independent. Indeed, this property is also in very good agreement with the numerics on the larger curvature model from Fig. 5, where the two data sets for $L=100$ and $L=120$ practically coincide.

Since the mean curvature depends on ϕ_4 only, for all cases below $z=5$ the dependence is given by the same formula (one just needs to replace the corresponding value for z).

(iv) $z = 3$. This is another borderline situation, and the leading time dependences are $U_q(L,t) \sim (\ln t)^{-1/2}$ and $\bar{U}(L,t) \sim (\ln t)^{-1/2}$.

(v) $1 < z < 3$. In this case the partition function and the density of minima all converge to a constant which to leading order is independent of the system size. The density of minima was shown in Sec. II to have this property in the steady state. Here we saw not only that, but also that *all* q moments show the same behavior, and, even more, the time behavior before reaching the steady-state constant is not a clean power law, but rather a decaying correction in the approach to this constant. The leading term in the temporal correction is $\sim t^{-(3-z)/z}$, and the next-to-leading term is $\sim t^{-(5-z)/z}$.

VI. CONCLUSIONS AND OUTLOOK

In summary, based on the analytical results presented, a short-wavelength analysis of interface fluctuations can pro-

vide us with interesting information and give an alternative description of surface morphologies. This analysis gives a more detailed characterization and can be used to distinguish interfaces that are “fuzzy” from those that locally appear to be smooth. The central quantities, the extremal-point densities, are numerically and analytically accessible. The partition-function-like formalism enables us to access a wide range of q moments of the local curvature distribution. In the case of the stochastic evolution equations studied, we could exactly relate these q moments to the structure function of the process via the simple quantities ϕ_2 and ϕ_4 . The wide spectrum of results accessed through this technique shows the richness of short-wavelength physics. This physics is there, and the long-wavelength approach simply cannot reproduce it, but instead may suggest an oversimplified picture of reality. For example, the MPEU model has been shown to belong in the steady state to the EW universality class; however, *it cannot be described exactly* by the EW equation in *all* respects, not even in the steady state. For example, the utilization (or density of minima) of the MPEU model is 0.24641, which for the EW model on a lattice is 0.25. Also, if one just simply looks at the steady-state configuration, one observes high *skewness* for the MPEU model [2], whereas the EW model is completely up-down symmetric. This can also be shown by comparing the calculated two-slope correlators. For a number of models that belong to the KPZ universality class, this broken-symmetry property compared to the EW case has recently received attention [2,35,36] and has been extensively investigated by Neergard and den Nijs [35]. The difference on the short-wavelength scale between two models that belong to the same universality class lies in the existence of irrelevant operators (in the renormalization group sense). Although these operators do not change universal properties, the quantities associated with them may be of very practical interest. The parallel computing example shows that the fundamental question of algorithmic scalability is answered based on the fact that the simulated time horizon in the steady state belongs to the EW universality class, and thus it has a *finite* density of local minima. The actual value of the density of local minima in the thermodynamic limit, however, strongly depends on the microscopic details, which in principle can be described in terms of irrelevant operators [35].

The extremal-point densities introduced in the present paper may actually have a broader application than stochastic surface fluctuations. The main geometrical characterization of fractal curves is based on the construction of their Hausdorff-Besikovich dimension, or the “box-counting” dimension: one covers the set with small boxes of linear size ϵ and then tracks the divergence of the number of boxes needed to cover in a minimal way the whole set as ϵ is lowered to zero. For example, a smooth line in the plane has a dimension of unity, but the Weierstrass curve of Eq. (2) has a dimension of $\ln b/\ln a$ (for $b > a$). The actual length of a fractal curve whose dimension is larger than unity diverges when $\epsilon \rightarrow 0^+$. The total length at a given resolution ϵ is a *global* property of the fractal; it does not tell us about the way it curves. The measure we propose in Eq. (3) is meant to characterize the distribution of a local property of the curve, its *bending*, which in turn is a measure of the curve’s wrinkledness. For simplicity we formulated it for functions,

i.e., for curves that are single valued in a certain direction. This can be remedied and generalized by introducing a parametrization $\gamma \in [0,1]$ of the curve, and then plotting the local *curvature* vs this parameter $K(\gamma)$. The plot will be a single-valued function on which Eq. (3) is easily defined.

Other desirable extensions of the present technique are (1) to include a statistical description of the degeneracies of higher order and (2) to repeat the analysis for higher (such as $d=2$) substrate dimensions. The latter promises an even richer spectrum of results, since in higher dimensions there is a plethora of singular points ($\nabla f = \mathbf{0}$) which are classified by the eigenvalues of the Hessian matrix of the function at the singular point. Deciphering the statistical behavior of these various singularities for randomly evolving surfaces is an interesting challenge. The studies performed by Kondev and Henley [37] on the distribution of contours on random Gaussian surfaces should be a good aid in achieving this goal. In particular, we may find the method developed here useful in studying the spin-glass ground state, and the spin-glass transition problem. (3) Another set of interesting extensions would be to analyze the effect of nonlinearities on the extremal-point densities. It is conceivable that in certain cases linear stochastic equations of type (87) will describe well only the long-wavelength limit, and the full description would in fact imply the existence of irrelevant nonlinear terms in the model. These nonlinearities are thus not affecting the universality class of the model but they perhaps can affect the critical value z_c at which the phase transition between the fuzzy and smooth behavior sets in. Last but not least, we invite the reader to consider, instead of the Langevin equations studied here, noisy wave equations, with a second derivative of the time component, or other stochastic evolution equations.

ACKNOWLEDGMENTS

We thank S. Benczik, M. E. Fisher, M. A. Novotny, P. A. Rikvold, Z. Rácz, B. Schmittmann, T. Tél, E. D. Williams, and I. Žutić for stimulating discussions. We are especially indebted to P. A. Rikvold for a critical reading of the manuscript. This work was supported by NSF-MRSEC at the University of Maryland, by DOE through SCRI-FSU, by NSF Grant Nos. DMR-9871455 and NSF-DMR-9727574, and by the Hungarian Science Foundation Grant No. F17166.

APPENDIX A: $\langle \Theta(-x_1)\Theta(x_2) \rangle$ FOR GENERAL COUPLED GAUSSIAN VARIABLES

The expression we derive in this Appendix, despite its simplicity, is probably the most important one concerning the extremal-point densities of one-dimensional Gaussian interfaces on a lattice. If the correlation matrix for two possibly coupled Gaussian variables is given by

$$\begin{aligned} \langle x_1^2 \rangle &= \langle x_2^2 \rangle = d > 0, \\ \langle x_1 x_2 \rangle &= c, \end{aligned} \quad (\text{A1})$$

then the distribution follows as

$$\begin{aligned} P(x_1, x_2) &= \frac{1}{2\pi\sqrt{\mathcal{D}}} \exp\left(-\frac{1}{2\mathcal{D}}(dx_1^2 + dx_2^2 - 2cx_1x_2)\right) \\ &= \frac{1}{2\pi\sqrt{\mathcal{D}}} \exp\left[-\frac{d}{2\mathcal{D}}\left(x_1^2 + x_2^2 - 2\frac{c}{d}x_1x_2\right)\right], \end{aligned} \quad (\text{A2})$$

where $\mathcal{D} \equiv d^2 - c^2 > 0$. We aim to find the average of the stochastic variable $u = \Theta(-x_1)\Theta(x_2)$:

$$\begin{aligned} \langle u \rangle &= \langle \Theta(-x_1)\Theta(x_2) \rangle = \int_{-\infty}^{\infty} \int_{-\infty}^{\infty} dx_1 dx_2 \\ &\quad \times \Theta(-x_1)\Theta(x_2)P(x_1, x_2), \end{aligned} \quad (\text{A3})$$

which is simply the total weight of the density $P(x_1, x_2)$ in the $x_1 < 0, x_2 > 0$ quadrant. If $c=0$, the density is isotropic, and $\langle u \rangle = 1/4$. In the general case it is convenient to find a new set of basis vectors where the probability density is isotropic (of course the shape of the original quadrant will transform accordingly). Introducing the linear transformation

$$\begin{aligned} x_1 &= \sqrt{\frac{\mathcal{D}}{2}} \left(\frac{y_1}{\sqrt{d+c}} + \frac{y_2}{\sqrt{d-c}} \right), \\ x_2 &= \sqrt{\frac{\mathcal{D}}{2}} \left(-\frac{y_1}{\sqrt{d+c}} + \frac{y_2}{\sqrt{d-c}} \right), \end{aligned} \quad (\text{A4})$$

and exploiting the fact that $\Theta(\lambda x) = \Theta(x)$ for $\lambda > 0$, we have

$$\begin{aligned} \langle u \rangle &= \int_{-\infty}^{\infty} \int_{-\infty}^{\infty} dy_1 dy_2 \Theta\left(-\frac{y_1}{\sqrt{d+c}} - \frac{y_2}{\sqrt{d-c}}\right) \Theta\left(-\frac{y_1}{\sqrt{d+c}}\right. \\ &\quad \left. + \frac{y_2}{\sqrt{d-c}}\right) \frac{1}{2\pi} \exp\left(-\frac{1}{2}(y_1^2 + y_2^2)\right). \end{aligned} \quad (\text{A5})$$

Now the probability density for the new variables y_1, y_2 is isotropic, and $\langle u \rangle = \theta/(2\pi)$, where θ is the angle enclosed by the two unit vectors

$$\mathbf{v}_1 = \frac{1}{\sqrt{2d}} \begin{pmatrix} -\sqrt{d+c} \\ \sqrt{d-c} \end{pmatrix}, \quad \mathbf{v}_2 = \frac{1}{\sqrt{2d}} \begin{pmatrix} -\sqrt{d+c} \\ -\sqrt{d-c} \end{pmatrix}. \quad (\text{A6})$$

From their dot product one obtains

$$\cos(\theta) = \frac{\mathbf{v}_1 \cdot \mathbf{v}_2}{|\mathbf{v}_1||\mathbf{v}_2|} = \frac{c}{d}, \quad (\text{A7})$$

and, thus, for $\langle u \rangle$,

$$\langle u \rangle = \frac{1}{2\pi} \arccos\left(\frac{c}{d}\right). \quad (\text{A8})$$

APPENDIX B: POISSON SUMMATION FORMULAS

In this Appendix we recall the well-known Poisson summation formula and adapt it for functions with finite support in \mathbb{R} . In the theory of generalized functions [38] the following identity is proven:

$$\sum_{m=-\infty}^{\infty} \delta(x-m) = \sum_{m=-\infty}^{\infty} e^{2\pi i m x}. \quad (\text{B1})$$

Let $f: [\alpha, \beta] \rightarrow \mathbb{R}$ be a continuous function with continuous derivative on the interval $[\alpha, \beta]$. Multiply Eq. (B1) on both sides by $f(x)$ and then integrate both sides from α to β . In the evaluation of the left-hand side we have to pay attention to whether either or both the numbers α and β are integers or nonintegers. In the integer case the contribution of the end point is calculated via the identity

$$\int_n^{n+r} dx \delta(x-n) f(x) = \frac{1}{2} f(n), \quad \forall r > 0. \quad (\text{B2})$$

Assuming that f is absolutely integrable if $\beta = \infty$, and choosing $\alpha = 0$, the classical Poisson summation formula is obtained:

$$\begin{aligned} \sum_{n=0}^{\infty} f(n) &= \frac{1}{2} f(0) + \int_0^{\infty} dx f(x) \\ &+ 2 \sum_{m=1}^{\infty} \int_0^{\infty} dx f(x) \cos(2\pi m x). \end{aligned} \quad (\text{B3})$$

Let us also write out explicitly the case when both α and β are integers:

$$\begin{aligned} \sum_{n=\alpha}^{\beta} f(n) &= \frac{1}{2} [f(\alpha) + f(\beta)] + \int_{\alpha}^{\beta} dx f(x) \\ &+ 2 \sum_{m=1}^{\infty} \int_{\alpha}^{\beta} dx f(x) \cos(2\pi m x) \quad \text{when } \alpha, \beta \in \mathbb{Z}. \end{aligned} \quad (\text{B4})$$

Next we apply these equations to give an exact closed expression for the slope correlation function for *finite* L [Eq. (18)]:

$$C_L^{\phi}(l) = \frac{D}{L} \sum_{n=1}^{L-1} \frac{e^{i(2\pi n/L)l}}{\nu + 2\kappa [1 - \cos(2\pi n/L)]}, \quad (\text{B5})$$

where $l \in \{0, 1, 2, \dots, L-1\}$, and $\nu, \kappa \in \mathbb{R}^+$. Let us denote

$$a = \frac{2\kappa}{\nu + 2\kappa}. \quad (\text{B6})$$

We have $|a| < 1$, and

$$C_L^{\phi}(l) = \frac{Da}{2\kappa L} \sum_{n=1}^{L-1} \frac{e^{i(2\pi n/L)l}}{1 - a \cos(2\pi n/L)}. \quad (\text{B7})$$

In order to apply the Poisson summation formula (B4), we introduce the function

$$f(x) = \frac{a}{2\kappa L} \sum_{n=1}^{L-1} \frac{e^{i(2\pi x/L)n}}{1 - a \cos(2\pi x/L)}, \quad 1 \leq x \leq L-1, \quad (\text{B8})$$

and identify in Eq. (B4) $\alpha \equiv 1$ and $\beta \equiv L-1$. The non-integral terms of Eq. (B4) give

$$\frac{1}{2} [f(1) + f(L-1)] = \frac{a}{2\kappa L} \frac{\cos[(2\pi/L)l]}{1 - a \cos[(2\pi/L)l]}. \quad (\text{B9})$$

The next term becomes

$$\begin{aligned} \int_1^{L-1} dx f(x) &= \frac{a}{2\kappa \sqrt{1-a^2}} \left(\frac{1 - \sqrt{1-a^2}}{a} \right)^l \\ &- \frac{a}{2\pi\kappa} \int_0^{2\pi/L} dx \frac{\cos xl}{1 - a \cos x}, \end{aligned} \quad (\text{B10})$$

where during the evaluation of the integral we made a simple change of variables and used a well-known integral from random-walk theory [10,34]:

$$\int_{-\pi}^{\pi} dx \frac{e^{ixl}}{1 - a \cos x} = \frac{2\pi}{\sqrt{1-a^2}} \left(\frac{1 - \sqrt{1-a^2}}{a} \right)^l, \quad l \geq 0. \quad (\text{B11})$$

The sum over the integrals in Eq. (B4) can also be evaluated, and one obtains

$$\begin{aligned} 2 \sum_{n=1}^{\infty} \int_1^{L-1} dx f(x) \cos(2\pi n x) &= \frac{a(b^l + b^{-l})}{2\kappa \sqrt{1-a^2}} \frac{b^L}{1-b^L} \\ &- \frac{a}{2\pi\kappa} \sum_{n=1}^{\infty} \int_{-2\pi/L}^{2\pi/L} dx \cos(nLx) \frac{e^{ilx}}{1 - a \cos x}, \end{aligned} \quad (\text{B12})$$

where

$$b = \frac{1 - \sqrt{1-a^2}}{a} \quad \text{and} \quad |b| < 1. \quad (\text{B13})$$

To compute the sum on the right-hand side of Eq. (B12), we recall another identity from the theory of generalized functions (see Ref. [38], p. 155):

$$\sum_{n=1}^{\infty} e^{inx} = \pi \sum_{m=-\infty}^{\infty} \delta(x - 2m\pi) + \frac{i}{2} \cot\left(\frac{x}{2}\right) - \frac{1}{2}. \quad (\text{B14})$$

Combining Eq. (B14) and identity (B1), one obtains:

$$\sum_{n=1}^{\infty} \cos(nx) = \pi \sum_{m=-\infty}^{\infty} \delta(x - 2m\pi) + \frac{1}{2}. \quad (\text{B15})$$

Performing the sum over n directly on the right-hand side of Eq. (B12) via Eq. (B15), yields

$$\begin{aligned}
& -\frac{a}{2\pi\kappa} \sum_{n=1}^{\infty} \int_{-2\pi/L}^{2\pi/L} dx \frac{\cos(nLx)e^{ilx}}{1-a\cos x} \\
& = -\frac{a}{2\kappa L} \sum_{m=-\infty}^{\infty} \int_{-2\pi}^{2\pi} dy \frac{e^{ily} \delta(y-2m\pi)}{1-a\cos y} \\
& \quad + \frac{a}{2\pi\kappa} \int_0^{2\pi/L} dx \frac{\cos lx}{1-a\cos x}. \tag{B16}
\end{aligned}$$

Only $m = \pm 1, 0$ contribute in Eq. (B16). With the help of Eq. (B2):

$$\begin{aligned}
& -\frac{a}{2\pi\kappa} \sum_{n=1}^{\infty} \int_{-2\pi/L}^{2\pi/L} dx \frac{\cos(nLx)e^{ilx}}{1-a\cos x} \\
& = -\frac{a}{2\kappa L} \left(\frac{1}{1-a} + \frac{\cos[(2\pi/L)l]}{1-a\cos(2\pi/L)} \right) \\
& \quad + \frac{a}{2\pi\kappa} \int_0^{2\pi/L} dx \frac{\cos lx}{1-a\cos x}. \tag{B17}
\end{aligned}$$

Using Eq. (B17) in Eq. (B12), we can add the result to the rest of the contributions (B9) and (B10) to obtain the final expression [Eq. (19)] after cancellations.

-
- [1] J. Krug and P. Meakin, *J. Phys. A* **23**, L987 (1990).
[2] G. Korniss, Z. Toroczkai, M. A. Novotny, and P. A. Rikvold, *Phys. Rev. Lett.* **84**, 1351 (2000).
[3] A. G. Greenberg, B. D. Lubachevsky, D. M. Nicol, and P. E. Wright, in *Proceedings, 8th Workshop on Parallel and Distributed Simulation (PADS '94), Edinburgh, U.K.*, edited by D. K. Arvind, R. Baprodia, and J. Y.-B. Lin (Society for Computer Simulations, San Diego, 1994), p. 187.
[4] G. Korniss, M. A. Novotny, and P. A. Rikvold, *J. Comput. Phys.* **153**, 488 (1999).
[5] M. B. Gorman, *J. Financial Econ.* **3**, 257 (1976).
[6] See, for example, <http://www.csuchico.edu/psy/BioPsych/neurotransmission.html>
[7] R. Albert, H. Jeong, and A.-L. Barabási, *Nature (London)* **401**, 130 (1999); A.-L. Barabási, R. Albert, and H. Jeong, *Physica A* **272**, 173 (1999); A.-L. Barabási and R. Albert, *Science* **286**, 509 (1999).
[8] G. H. Hardy, *Trans. Am. Math. Soc.* **17**, 301 (1916).
[9] B. R. Hunt, *Proc. Am. Math. Soc.* **126**, 791 (1998).
[10] B. D. Hughes, *Random Walks and Random Environments, Volume 1: Random Walks* (Clarendon Press, Oxford, 1995).
[11] D. Ruelle, *Thermodynamic Formalism* (Addison-Wesley, Reading, MA, 1978); T. Bohr and D. Rand, *Physica D* **25**, 387 (1987).
[12] H.-C. Jeong and E. D. Williams, *Surf. Sci. Rep.* **34**, 171 (1999).
[13] M. Giesen and G. S. Icking-Konert, *Surf. Sci.* **412/413**, 645 (1998).
[14] Z. Toroczkai and E. D. Williams, *Phys. Today* **52**(12), 24 (1999).
[15] S. V. Khare and T. L. Einstein, *Phys. Rev. B* **57**, 4782 (1998).
[16] A.-L. Barabási and H. E. Stanley, *Fractal Concepts in Surface Growth* (Cambridge University Press, Cambridge, 1995).
[17] J. Krug, *Adv. Phys.* **46**, 137 (1997); S. Das Sarma, C. J. Lanczycki, R. Kotlyar, and S. V. Ghaisas, *Phys. Rev. E* **53**, 359 (1996).
[18] J. Villain, *J. Phys. I* **1**, 19 (1991); Z. W. Lai and S. Das Sarma, *Phys. Rev. Lett.* **66**, 2348 (1991); D. D. Vvedensky, A. Zangwill, C. N. Luse, and M. R. Wilby, *Phys. Rev. E* **48**, 852 (1993).
[19] S. Das Sarma and P. Tamborenea, *Phys. Rev. Lett.* **66**, 325 (1991); D. E. Wolf and J. Villain, *Europhys. Lett.* **13**, 389 (1990).
[20] S. Majaniemi, T. Ala-Nissila, and J. Krug, *Phys. Rev. B* **53**, 8071 (1996).
[21] W. W. Mullins, *J. Appl. Phys.* **28**, 333 (1957); **30**, 77 (1957); in *Metal Surfaces*, edited by W. D. Robertson and N. A. Gjostein (American Society of Metals, Metals Park, OH, 1962), p. 17.
[22] S. F. Edwards and D. R. Wilkinson, *Proc. R. Soc. London, Ser. A* **381**, 17 (1982).
[23] M. Kardar, G. Parisi, and Y.-C. Zhang, *Phys. Rev. Lett.* **56**, 889 (1986).
[24] P. Meakin, P. Ramanlal, L. M. Sander, and R. C. Ball, *Phys. Rev. A* **34**, 5091 (1986); M. Plischke, Z. Rácz, and D. Liu, *Phys. Rev. B* **35**, 3485 (1987); L. M. Sander and H. Yan, *Phys. Rev. A* **44**, 4885 (1991).
[25] F. Spitzer, *Adv. Math.* **5**, 246 (1970).
[26] R. M. Fujimoto, *Commun. ACM* **33**, 30 (1990).
[27] B. D. Lubachevsky, *Complex Syst.* **1**, 1099 (1987); *J. Comput. Phys.* **75**, 103 (1988).
[28] A. G. Greenberg, S. Shenker, and A. L. Stolyar, *Performance Eval. Rev.* **24**, 91 (1996).
[29] B. Bruisma, in *Surface Disordering: Growth, Roughening and Phase Transitions*, edited by R. Jullien, J. Kertész, P. Meakin, and D. E. Wolf (Nova Science, New York, 1992).
[30] J. M. Kim and S. Das Sarma, *Phys. Rev. Lett.* **72**, 2903 (1994).
[31] J. Krug, *Phys. Rev. Lett.* **72**, 2907 (1994).
[32] J. G. Amar, P.-M. Lam, and F. Family, *Phys. Rev. E* **47**, 3242 (1993); M. Siegert and M. Plischke, *Phys. Rev. Lett.* **68**, 2035 (1992).
[33] C. Itzykson and J.-M. Drouffe, *Statistical Field Theory* (Cambridge University Press, 1989), Vol. 1.
[34] I. S. Gradshteyn and I. M. Ryzhik, *Table of Integrals, Series, and Products*, edited by Alan Jeffrey (Academic Press, New York, 1994).
[35] J. Neergard and M. den Nijs, *J. Phys. A* **30**, 1935 (1997).
[36] P. A. Rikvold and M. Kolesik, *J. Stat. Phys.* (to be published); e-print cond-mat/9909188.
[37] J. Kondev and C. L. Henley, *Phys. Rev. Lett.* **74**, 4580 (1995).
[38] D. S. Jones, *The Theory of Generalized Functions* (Cambridge University Press, Cambridge, 1982), p. 153.